Conformation-dependent conductance in single molecular break junctions

by

Joseph Martin Hamill

(Under the direction of Bingqian Xu)

Abstract

Force and conductance, measured across 4,4'-bipyridine simultaneously, are crosscorrelated using a two dimensional (2D) histogram method. The result is a 2D multivariate statistical analysis superior to current one dimensional histogram techniques for exploring significant conductance and force modulations within SMBJs. This method is sensitive enough to cross-correlate signal modulations between force and conductance traces associated with contact geometry perturbations predicted in literature such as Au-molecule contact twisting and slipping during junction elongation. Additionally, this technique is simple enough to use out-of-the-box, illustrated by its application in DNA conductance measurements to describe junction conformation, facilitating better understanding of the system.

Index words: Single molecular break junctions, scanning probe microscopy, conducting atomic force microscopy

Conformation-dependent conductance in single molecular break junctions

by

Joseph Martin Hamill

B.S., Western Washington University, 2007

A Thesis Submitted to the Graduate Faculty

of The University of Georgia in Partial Fulfillment

of the

Requirements for the Degree

Masters

Athens, Georgia

2014

Conformation-dependent conductance in single molecular break junctions

by

Joseph Martin Hamill

Approved:

Major Professor: Bingqian Xu

Committee: Henry F. Schaefer III
Peter Kner

Electronic Version Approved:

Julie Coffield
Interim Dean of the Graduate School
The University of Georgia
August 2014

Acknowledgments

Thanks to the giant spaghetti monster.

Table of Contents

Acknowledgments **iv**

1 Introduction **1**

1.1 Summary 1

1.2 Methods 3

1.3 Concluding remarks 4

2 Literature Review: Characterizing molecular junctions through the MCBJ approach **7**

2.1 Abstract 8

2.2 Introduction 8

2.3 MCBJ experimental challenges 9

2.4 Importance of Contact Geometry and Evolution in MCBJs . . . 15

2.5 Theoretical advancements in electrochemical redox experiments 16

2.6 The role of external bias 19

2.7 Environmental influences 20

2.8 Conclusion and Outlook 23

3 Force and conductance molecular break junctions with time series crosscorrelation **26**

3.1 Abstract 27

3.2 Introduction 27
3.3 Results and Discussion 29
3.4 Conclusion 43

4 Conclusion **44**
4.1 A Review of the past with an eye on the future 44
4.2 An Experiment with future potential 44
4.3 Final thoughts 45

Bibliography **46**

Appendices **58**

Appendix A 2D Correlation Histogram Algorithm **58**
A.1 Pearson's Correlation Coefficient 58

Chapter 1

Introduction

1.1 Summary

A molecule contacted by two metal electrodes, a single molecular break junction (SMBJ), provides a platform to study the chemical, mechanical, and electrical properties of individual molecules in a quasi-isolated setting. Using SMBJs, molecules can be explored for unique applications in optoelectronics, spintronics, and other uses in nanoelectronics. The uniqueness of a molecule's behavior in a SMBJ comes from the nonlinear dependence of conductance on the conformation of the molecule-electrode coupling. The goal of this study is to better understand the correlation between conformation and conductance in metal-molecule-metal junctions. A SMBJ produces an ensemble of metal-molecule-metal junctions in succession by opening and closing metal electrodes repeatedly when a molecule with metal-interacting end groups is present between the electrodes. By applying a bias across the electrodes, the conductance of the SMBJ can be measured and information about the electrical properties of the molecule can be derived.[1–3] Multiple molecules over the past two decades have been studied in SMBJs, and the results are confident techniques for controlling the orientation of the molecule within the junction, and for analyzing the data to determine the single molecular conductance.[4,5] Today it is better understood that the physical conformation of the molecule and the electrodes play leading roles in determining the conductance of SMBJs.[6,7]

The goal of this thesis is to systematically study the effects on SMBJ conductance caused by conformation changes in the molecule and the electrodes using data analysis techniques. This paper will cover mostly the details of a 4,4'-bipyridine junction, but will draw upon lessons learned from two separate DNA experiments as well:

1. Ch. 3 covers a proof of concept for a new SMBJ data analysis technique based on Pearson's crosscorrelation. 4,4-bipyridine (4,4'bpy) will be measured in a C-AFM SPMBJ which will simultaneously measure force and conductance while the junction elongates and breaks. Because 4,4'bpy is a stiff aromatic molecule, the conformation change in this junction will come predominantly from the metal-metal bonds in the electrodes.[3,8–15] This molecule has been studied many times before, however time series crosscorrelation between force and conductance is a new technique which facilitates understanding about the forced conformation changes in the junction and correlates these changes with changes in conductance.

2. To better understand the 4,4'bpy analysis results, the same algorithm has been used on a DNA experiment and included in section 3.3.1.1. This experiment studies the effects of altering the conformation of short sequence double stranded DNA. The concentration of cations in the DNA buffer will be increased, which has been shown in literature to alter the twist angle and separation of the bases in DNA.[16–22] By functionalizing the 5' end of each ssDNA it will be possible to deposit a monolayer of DNA molecules on the Au surface while the opposite thiolated 5' end is oriented vertically to interact with the Au STM tip.

1.2 Methods

1.2.1 Scanning probe microscopy break junctions

A scanning tunneling microscope (STM) can be operated as a probe to contact and manipulate individual molecules.[3] This technique is called scanning probe microscopy break junction (SPMBJ). This technique has proven very successful at creating SMBJs. The SPMBJ technique has also been effective using conducting atomic force microscopy (C-AFM), replacing the STM tip with a conducting AFM cantilever. Ch. 2 provides an overview of the history and current state of the art of SPMBJ techniques.

1.2.2 C-AFM for force-conductance crosscorrelation

Conducting atomic force microscopy (C-AFM)[14] will be used as a SPMBJ device to simultaneously measure force alongside conductance. 4,4'bpy will be studied using C-AFM SPMBJ because it will remain rigid allowing the conformation changes in the metal electrodes to be measured. Using the SPMBJ technique it will be possible to observe and record these mechanical and electronic changes with an oscilloscope and finally with LabVIEW software to analyze the signal. Data analysis methods beyond the usual 1D conductance histogram will then be employed. Recent advancements in data analysis methods provide new abilities to derive physical information about the SMBJ system.

1.2.3 STM for DNA-Mg^{2+} conductance

A STM probe will be used to manipulate DNA molecules. To alter the conformation of short stranded DNA, the buffer solution of a sequence of dsDNA poly[d$(CG)_4$] will contain various concentrations of $MgCl_2$. By varying the concentration of ions in the buffer, the

conformation of the dsDNA can be altered, studied, and compared. It is possible this will induce a discrete transition to Z-DNA, instead of a continuous conformation change of the B-DNA.

1.2.4 Two dimensional crosscorrelation histograms

The 4,4'bpy C-AFM experiment in Ch. 3 will be used as a test bed for a new data analysis algorithm to calculate crosscorrelation between time series force and conductance measurements. Although not a true time-dependent calculation, it provides a proof of concept that time series analysis (TSA) techniques can and should be applied to SPMBJ measurements as a way of deriving relationships between conformation changes and conductance changes. This dependency is understood to be the driving cause of conductance modulations in SPMBJ measurements.

Recent literature has shown the effectiveness of the prototype utilizing autocorrelation of conductance SPMBJ measurements alone.[23] Other work has shown the growing desire for a force-conductance crosscorrelation analysis technique to better understand conformation changes in SPMBJs.[24–26] The algorithm used by Makk, *et al* follows closely to Pearson's formula for autocorrelation (Eq. (3.1) for multiple time-dependent samples of a single variable. The flow chart in Fig. 1.1 depicts this algorithm. To extend this algorithm to two variables, the left column replaces conductance traces by force traces as in Fig. 1.2. Nothing new is derived here, because this is merely Pearson's formula for crosscorrelation (Eq. 3.4). A more detailed discussion of the algorithm can be found in Appendix A.

1.3 Concluding remarks

Confidence is growing in the procedures involved in SPMBJ techniques. It is now time to apply more sophisticated statistical analysis techniques to derive higher resolution information from the data garnered from these measurements. Time series analysis is a powerful toolbox

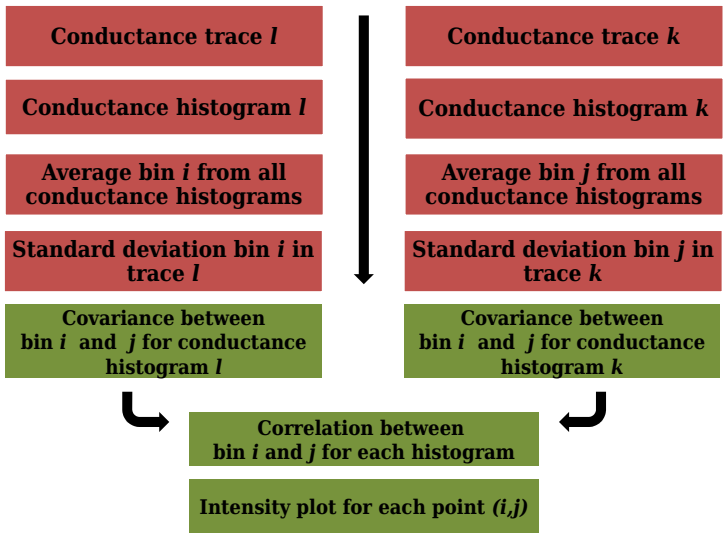

Figure 1.1: Flow chart of pseudocode for calculating autocorrelation from multiple time-dependent samples.

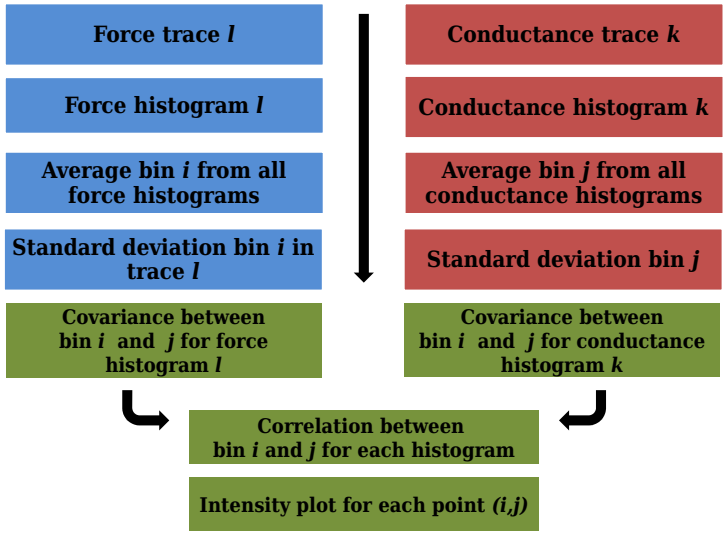

Figure 1.2: Flow chart of pseudocode for calculating crosscorrelation from multiple time-dependent samples.

ready-made to glean as much information as possible, to the finest resolution possible, from time-dependent dynamic processes such as those processes occurring within a SMBJ. With the appropriate application of statistical methods, it will be possible to distinguish modulations within SMBJ data and correlate them to perturbations due to conformation changes during elongation of the junction. Another consequence of the confidence in the SPM SMBJ techniques is the ability to use this tool in cooperation with other tools. Already such tools include optical[27–29] and force[14] measurements. These are measured simultaneously alongside conductance measurements. This form of multivariate analysis provides even more advanced capabilities for time series analysis in two dimensional crosscorrelation calculations. But first the consequences of various conformation changes must be understood. Therefore, systematic studies of controlled conformation changes must be accomplished before the signals within dynamic systems can be identified. This project hopes to achieve each of these necessary studies: two studies of conformation change in a molecule, and one study of dynamic electrode conformation change during junction elongation. Elementary time series analysis techniques will be utilized to show the usefulness of this new approach to SPM SMBJ data analysis in hopes that more advanced algorithms can be applied in the future.

Chapter 2

Literature Review:

Characterizing molecular junctions through the MCBJ approach*

*J.M. Hamill, K. Wang, B. Xu. 2014. *Reports in Electrochemisty.* **4**:1-11 (2014). Reprinted here with permission of the publisher.

2.1 Abstract

Mechanically controlled break junction (MCBJ) techniques, which emerged right after the invention of scanning tunneling microscopy, have enabled substantial progress in characterizing single-molecule junctions towards the ultimate goal of molecular devices. Dramatic advances have been made in design, fabrication, control, and understanding of the measurements of single-molecule junctions over the past decade. In this overview we present the evolution of some of the recent issues, and an outlook for further developments in MCBJ techniques for characterizing molecular junctions. Topics of recent interest include: contact geometry, electrochemical redox experiments, external bias effect, and environmental influences. Each will need further investigation to thoroughly understand the experimental information revealed from a molecular junction.

2.2 Introduction

The desire to overcome the prediction of Moores Law led researchers to single-molecule scale devices.[30–32] Molecular junctions emerged from the late 90s,[1] catalyzed by the invention of scanning tunneling microscopy (STM) and inspired by a paper by Aviram and Ratner describing molecular sized p-n junctions.[33,34] In the search for effective ways to couple a molecule between electrodes, researchers produced two efficient options: scan-ning probe microscopy (SPM) using the newly invented STM, and a micro-fabricated, electromigration piezoelectric three-point arching method. Both techniques provided a reli-able platform to conduct measurements at a single-molecule level by utilizing piezoelectric transducers to mechanically open and close a break junction in which a molecule had be-come bonded. The key features of each of these methods, and all other mechanically con-trolled break junctions (MCBJs) is a molecule in contact with two or more electrodes where one of the electrodes is mechanically controlled to allow it to create, break, and reform junctions with the molecule

incorporated. In this way, the four main features of study in MCBJs are 1) the electrodes (and the macroscopic system), 2) the electrode-molecule junction, 3) the molecule, and 4) the environment in which the junction takes place. Often this environment is in solution,[1,3] sometimes in vacuum,[35–37] and sometimes at cryogenic temperatures.[38–40]

The methods of MCBJs have come a long way since the early stages of the last decades. Experiments using MCBJs to measure the conductance of single molecules began in earnest in the late 90s and the first years of experiments resulted in many discrepancies among the measured and simulated results of single molecular conductance from different labs. As the techniques matured, and as more labs took part in the experiments, the re-producibility of MCBJ experiments became more reliable.[5] Today MCBJ techniques are used in conjunction with other measurement techniques,[28,41] either simultaneously or back to back, to derive still more information about the behavior of molecules at the nanoscopic level.

Some of the more detailed challenges that troubled the field in those early years, such as the strong sensitivity of MCBJs to contact geometry, behaviors relating to redox reac-tions in molecules in MCBJs, and the phenomenon of negative differential resistance (NDR) as well as other nonlinear current-voltage behaviors of molecular junctions have been studied at length in the last decade, and we know much more about these issues to-day. We hope to discuss these advancements here as well as discuss new directions for the future.

2.3 MCBJ experimental challenges

Before anything resembling single molecular electronics becomes possible, reliable molecule-electrode junctions using chemical bonds are essential. Without these, it had been necessary to rely on approaching the molecule within proximity to the electrodes using increasingly clever ways: using mercury drops as electrodes,[42] using Lorentz force to cross metallic wires,[43] and trapping molecules in a nanopore.[44,45] Other successful techniques involved sandwiching the ends of very robust molecules between layers of electrode material, usually by thermal

evaporation, and using lithographic techniques to etch away undesirable quantities of the substrate and electrodesthese techniques worked great for long and strong carbon nanotubes (CNTs), but are too destructive for smaller molecules.[46] A different method involved criss-crossing nanowires by overlaying layer after layer. This, however, usually only produced large arrays of nanojunctions: the single molecular junction was still out of reach.[47,48] It was still necessary to find ways to bond one end of the molecule to one electrode, the other end to the second electrode.

Ways to chemically bond the molecule to the electrodes were finally developed using amine and thiol functionalized molecules which bond readily to metal electrodes. Thiol functionalized molecules were used in the crossed-wire technique,[49] and the first attempts to use a STM to probe molecular conductance were attempted by functionalizing one side of the molecule, and scanning the other end in a traditional STM or conducting atomic force microscopy (C-AFM) method,[50,51] or with the probe scanning a gold nanoparticle atop the molecule.[52,53] Finally, both ends of the molecule were functionalized and successfully incorporated into a mechanical break junction. One of the first truly powerful break junction techniques used a piezoelectric transducer to arch a platform onto which a metallic wire had been anchored.[1] By lithographically etching the metallic wire until it was nanoscopically thin, the arching of the platform allowed complete control of the breaking and reforming of nanojunctions repeatedly with sub-angstrom control.[54,55] This three-point arching technique provides experimentalists today with a way to perform complementary measurements, such as optical spectroscopy, alongside MCBJ conductance measure-ments because the design of the apparatus leaves the top exposed.[56–58]

Another powerful method for creating MCBJs was created by Xu and Tao.[3] This method involved smashing a gold tip into a gold substrate (Fig. 2.1A) starting from a traditional STM setup, where a liquid cell was placed such that the molecule in solution was on top of the gold substrate. When the gold tip was withdrawn, many molecules were incorporated

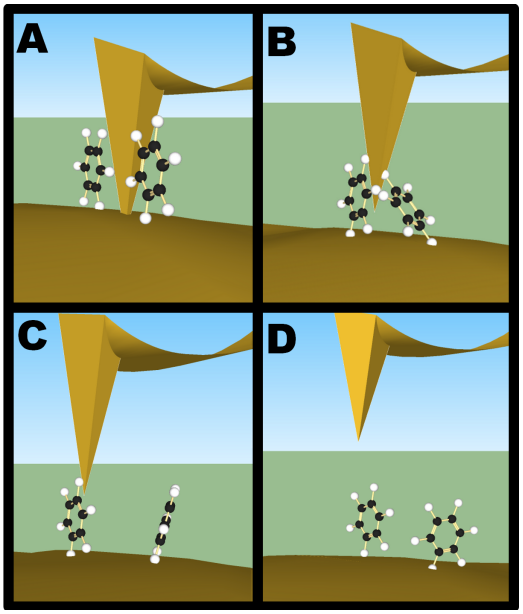

Figure 2.1: Time lapse of conductance atomic force microscopy (C-AFM) single molecular break junction. An identical process occurs with a scanning tunneling microscope tip replacing the C-AFM cantilever. (A) Au coated C-AFM cantilever collides with Au coated substrate until a conductance of many conductance quanta are registered indicating a large contact surface between cantilever and substrate. (B) The cantilever is retracted leaving multiple molecules in the junction. (C) The cantilever continues to retract until a single molecule is in the junction. (D) The cantilever retracts until the conductance represents the vacuum current and then the process is repeated.

into the gap between the tip and substrate (Fig. 2.1B), but as the tip was withdrawn further, the molecules broke one-by-one until there was only one left in the break junction (Fig. 2.1C). All the while, a bias was applied between the tip and the substrate and the current across the junction was recorded. As the molecules broke away, individual steps in the conductance were observed, each step differing from the next by a unique value of conductance. For atomically thin metal junctions, these quantized steps were predicted, and experimentally shown, to have a conductance of $G_0 = n * 2e^2h^{-1}$, where n is an integer, e is the electronic charge, and h is Plancks constant.[59] After the last metallic junction, new steps were observed for conductance values much smaller than the conductance quantum of G_0. These steps corresponded to integer numbers of molecules in the junction. The last step before the conductance fell to zero (Fig. 2.1D) was the conductance across a single molecule.

Creating strong bonds with the gold electrode at both junctions was a significant improvement upon the previous methods, and created clear data (Figs. 2.2A-D). Proving the molecule, in this case a 4,4-bipyridine molecule, was indeed present in the junction was the next task. The new SPM technique developed by Xu and Tao was very destructive, because it involved smashing the STM tip into the substrate before withdrawing it, and it was necessary to prove that, during the withdrawal, a substrate-molecule-tip junction was indeed formed. Because the nitrogen was located at either end of the 4,4-bipyridine molecule it was able to bond simultaneously with both electrodes. By conducting the SPM measurement in solution without the molecule present, it was trivial to show that the conductance fell off exponentially, without the presence of the signature steps at the conductance of the molecule (Figs. 2.2E-F). Next, 2,2-bipyridine was measured in solution. Because the nitrogen in 2,2-bipyridine is not located at the end of the rod-like aromatic rings, it was not possible for it to bond simultaneously to both electrodes, and the conduct-ance could not be measured, resulting once again with conductance traces that fell off ex-ponentially without steps. Because there was much thermal noise in measurements of this precision,[61] it was beneficial to

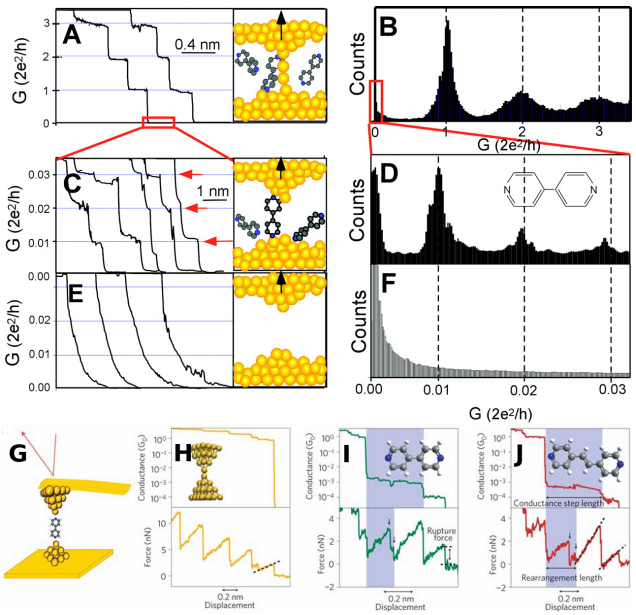

Figure 2.2: Representative MCBJ data. (A) Au-Au junction conductance trace with quantized conductance of step G_0. (B) Conductance histogram from Au-Au conductance traces. (C) Au-4,4-bipyridine-Au junction conductance traces with quantized conductance step 0.01 G_0. (D) Conductance histogram from multiple traces. (E) Conductance traces without molecule present with no quantized steps. (F) Conductance histogram without peaks. (G) Conducting atomic force microscopy schematic (C-AFM). (H) Example Au-Au junction conductance (note semi-logarithmic scale for following conductance traces) and force traces resulting from C-AFM . (I) Example traces for 4,4-bipyridine junction. (J) Example traces for 1,2-bis(4-pyridyl)ethylene junction. (A)-(F) Reprinted with permission from the publisher. Measurement of single-molecule resistance by repeated formation of molecular junctions. *Science*. 2003;301(5637):12211223. ©2003 American Association for the Advancement of Science.[3] (G)-(J) Reprinted by permission from Macmillan Publishers Ltd: *Nat Mater*, Aradhya SV, Frei M, Hybertsen MS, Venkataraman L. Van der Waals interactions at metal/organic interfaces at the single-molecule level. 2012;11(10):872876. Copyright 2012.[60]

create 1D histograms which revealed the statistical average of single molecular conductance over thousands of repeated measurements (Fig. 2.2B and 2.2D).[62,63] Despite the reliance on statistical methods, this new SPMBJ technique resolved many standing debates surrounding MCBJs. SPMBJs showed that short strands of DNA can be described most accurately as a semiconductor.[64] Up until this point, there was much debate surrounding the electronic properties of DNA, with proponents arguing for insulator,[65] large band gap semiconductor,[66] conductor,[67,68] and even superconductor.[69] SPMBJs showed that, especially for short strands heavy in guanine, DNA acted very much like a semiconductor.[64]

Reviews from the field of MCBJ written in the first decade of the 21st century all had one concern in common: reproducibility.[2,5,70] The SPMBJ technique resolved yet another debate, by confidently and repeatedly measuring the conductance of simple alkanedithiol chains, molecules which up until that point had discrepancies between different labs, and between theory and experiment.[3,71,72] Experiments on the single molecular conductance of octanedithiol conducted at different labs in 2001,[73] 2003,[3] and 2004[74] appeared to have widely ranging results. After closer attention, these discrepancies have been resolved.[5]

As is so common in science, the resolution of one concern often is accompanied by new insight into other concerns. The resolution of the discrepancy in octanedithiol single molecular conductance provided important information about the significance of contact geometry in MCBJs. It was shown that when the molecule is contacted to a planar crystalline electrode, it is of only minor importance whether it is contacted in a hill or valley of the crystal. Of significantly more importance is a contact geometry in which the molecule contacts a pyramidal shaped crystalline electrode instead of a planar electrode. In the pyrami-dal case the conductance is greatly decreased when compared to the planar case. Thus if the experimental apparatus has a preference for creating one contact geometry over another, than this can explain why different apparatus produce different single molecular conductance values.

2.4 Importance of Contact Geometry and Evolution in MCBJs

At the most basic level, progress in controlling physical and chemical properties of a molecular junction started with the capability of making robust contact to form a single-molecule junction. This proving a difficult task, the role of the contact interfaces was omit-ted at the initial time point. Experiments without careful control of the contact parts revealed data hard to interpret.[75,76]

It has recently become apparent that electrode geometry and specific orientation at which the molecule contacts the electrodes has a profound influence on the behavior of MCBJ measurements, and much effort has been devoted to understanding this phenome-non. Detailed quantum chemical studies have even shown allowed and forbidden states, based on phase and symmetry groups, influence molecular conductance.[36,77]

C-AFM (Figure 2G) is especially useful in measuring contact changes and flexibility during MCBJs. C-AFM uses a similar method as SPMBJs, but replaces the STM tip with an AFM cantilever. The result is a MCBJ in which force can be measured alongside conductance (Figs. 2.2H- 2.2J).[78] This technique was used to study contact phenomenon such as local heating, where it was predicted that inelastic scattering of electrons caused an in-crease in the temperature of the molecule.[79,80] It has also shown that gold contacts in a tetrahedral crystal structure have a quantized length slipping, allowing one, two, and three simultaneous slip events for each of the three tetrahedral faces slipping individually.[81]

Theoretical formalism describes the MCBJ system as a quantum scattering event with the molecule in the junction performing the scattering much like any dielectric material.[59,82] In this interpretation the mechanism by which electrons are delivered to the junction via the contacts is of major significance, even when compared to the significance of the molecule in the junction. As stated above, the shape of the electrode where it contacts the molecule is of paramount importance. But a MCBJ is a dynamic event which undergoes mechanical

stretching, thermal fluctuations,[83] local current-induced heating,[78,80] and redox reactions.[84] With this in mind, researchers have been focusing much attention on the progression of the MCBJ as it is formed, stretched, and finally broken. Computer simulations have been of immense help in this area because, as of yet, direct observation of contact geometry evolution in experiments has been difficult.[10,25] Simulations reported that with the same molecule bridged between electrodes with different shape reveal totally different I-V characteristics and asymmetric binding sites of the anchoring group could also influence the resulting electronic properties.[6,85,86] The same molecule can even have two or more probably orientations within a junction, each with a unique conductance signature (Fig. 2.3A).[60]

The conductance across MCBJs as tunneling electron microscopy (TEM) images are taken show, as multiple atoms are individually added to the chain, the conductance oscillates in a consistent manner.[25,87–90] Careful studies of similar chains occurring when a mol-ecule is present in the junction have shown that metal chains of four atoms long can occur before the junction breaks.[13] Other simulation work have shown the effects of slipping gold-gold bonds (Figs. 2.3B and 2.3C), and molecule-electrode slipping (Figs. 2.3D and 2.3E) and twisting (Figs. 2.3F and 2.3G) on the conductance in MCBJs.[7,11] Studies like this reveal the molecular MCBJ to be flexible at the electrode junction, and this geometric flexibility has significant influence on the molecular conductance as the junction evolves during the process of breaking. Some phenomena predicted for molecular electronics, it has been suggested, require this flexibility, and more.[91] In cases where the junction is required to stretch still further, CNTs have been suggested.[92]

2.5 Theoretical advancements in electrochemical redox experiments

Most often the overarching goal of MCBJ research is to understand and control the alignment of the molecules Fermi level with the conducting molecular orbitals (MOs) of the electrodes: the highest occupied molecular orbital (HOMO) for hole transfer, and the lowest unoccu-

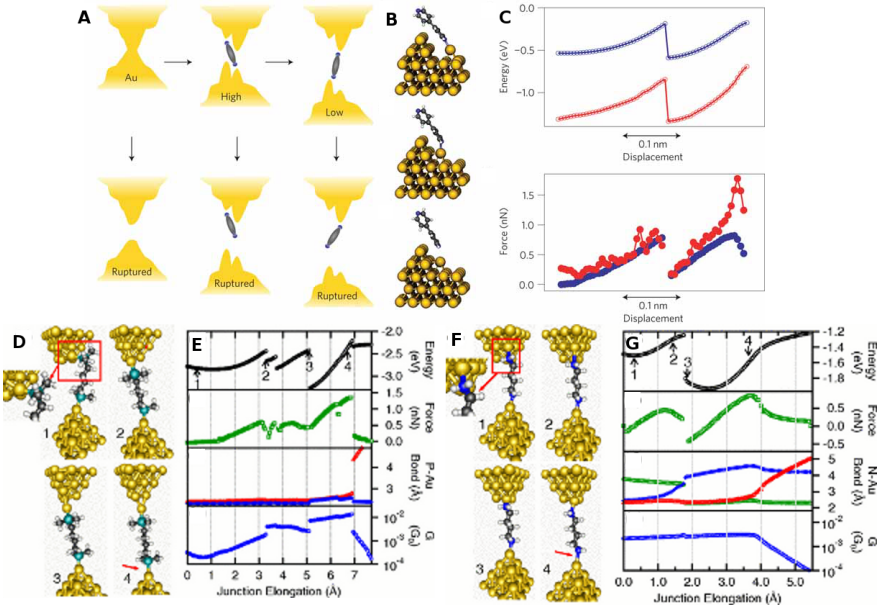

Figure 2.3: Example of geometric adjustments during MCBJ elongation. (A) 4,4-bipyridine orients in two ways during junction elongation resulting in two separate values for conductance. (B) Example slip of Au-Au bond. (C) Simulated changes in energy and force due to Au-Au bond slip. (D) Example slip of P-Au bond. (E) Simulated changes in energy, force, bond length, and conductance due to P-Au bond slip. (F) Example N-Au bond twist. (G) Simulated changes in energy, force, bond length, and conductance due to N-Au bond twist. (A)-(C) Reprinted by permission from Macmillan Publishers Ltd: *Nat Mater,* Aradhya SV, Frei M, Hybertsen MS, Venkataraman L. Van der Waals interactions at metal/organic interfaces at the single-molecule level. 2012;11(10):872876. Copyright 2012.[60] (D)-(G) Reprinted from figure with permission from Kamenetska M, Koentopp M, Whalley AC, et al. *Phys Rev Lett*, 102, 126803, 2009. ©2009 by the American Physical Society.[7]

pied molecular orbital (LUMO) for electron transfer.[93] Electrochemical gating of molecular conductance due to redox reactions is possibly the most powerful method to control this alignment.[94–98] Adding a third terminal to the electrolytic solution within the liquid cell containing the MCBJ allows the experimentalist great control over the local potential at the molecule. For junctions with a large HOMO-LUMO gap, this gating has shown little effect because the Fermi level of the molecule was never able to reach the conducting MOs.[99] Some molecules exhibited reduction of nitrite groups, and although conductance was significantly increased when negative bias was applied to the gating terminal, the re-action was irreversible. The reaction did have the effect of causing a rectification feature in the current-bias (I-V) relationship of the molecule, and the reaction also caused negative differential resistance (NDR) phenomenon.[100] Of far greater interest were molecules which experienced reversible redox reactions, thus allowing the molecule to be gated on and off resulting in ranges of conductance of as much as 15 magnitudes.[101] Cyclic voltammetry revealed that the molecule switched between a low-conductance reduced state to a high-conductance oxidized state.[102] There was great control over this reaction, however stochastic switching between states was also observed. For most molecules, high bias is required to maintain one state or the other.[5]

Recently, transition voltage spectroscopy (TVS)[103] was used to calculate the energy gap between the molecular Fermi level and the nearest frontier molecular orbital (FMOs) in order to quantitatively show that the solution in which the molecule is immersed contributes to electron transfer, helping resolve questions about the role of solvent in MCBJs.[3,104,105] In conjunction with a simplified model and the electrochemical techniques described in the previous paragraph, TVS was helpful in showing the effects of electrochemical gating on single molecular conductance.[106] The TVS approach was also helpful in comparing the relative importance of molecular length,[107] contact geometry, energy level alignment, and contact resistance, and showed that contact resistance is the dominant factor in mechanical

break junction conductance.[108] TVS can discern between the effects of Schottky barriers versus defect barriers at the molecule-electrode junctions.[109] TVS analy-sis on experimental data, along with density function theory simulations, identified the MOs, not merely the HOMO and LUMO, responsible for electron transport, and furthermore showed that these MOs can change as the probe-substrate distance is varied.[110] TVS has shown potential to address many questions surrounding MCBJs, even while presenting new questions.[111,112]

2.6 The role of external bias

Since the electronic properties of a molecular junction, such as conductance and I-V characteristics, has to be measured under an external bias applied on one of the electrodes, this bias plays a prominent role in affecting the charge transport process across the junction. Many studies have emphasized the importance of the explicit inclusion of bias effect in explaining the electrical results of molecular junctions.[6,113] Given that the static conductance is usually measured under a fixed bias, I-V characteristics measured using a bias sweep is the key feature which reflects the influence of external bias. Rectification be-havior and NDR have been studied as the main focus of molecular electronics, since the asymmetric current at the same bias magnitude, but opposite bias polarity, is the first step to ultimately realizing a molecular diode. To date, in most molecular rectification studies with MCBJ, the switch-on voltage, where rectification ratio starts going beyond unity, is postponed to a certain bias voltage[38,86,114–116] instead of the ideal case for bulk diode, where the switch-on voltage is close to zero. Certain rectifying molecules do show immediate switch-on.[117] Pati *et al* reported an electron-phonon interaction mode perpendicular to the direction of current flow which increases with the increase of external bias, and in turn destroyed part of the electrode-molecule-electrode current.[6] Other simulations[6,118] based on the transmission function, suggested that the FMOs and the MOs away from the Fermi energy of the electrode

respond differently to the applied bias: the transmission peaks may rise, fall and shift as the bias increases (Figs. 2.4A and 2.4C). All the effects induced by external bias were responsible for resulting electrical measurement properties.

NDR, defined as a non-monotonic dependence of current on the bias voltage (for example, the current decreases with increasing bias), has been observed for various metal-molecule-metal junctions.[44,119–122] But the sources of this effect are still in controversy. The main sources are discussed to be bias-dependent electron-phonon interaction, potential-drop-induced shifting of MOs, nonlinear bias-dependent effective coupling between MOs and the electrodes (Fig. 2.4B), and even image-charge effects. All possible mechanisms involve the significance of external applied bias.

2.7 Environmental influences

Besides the structure of a molecular junction, effects from the environment surround-ing the MCBJ have been of considerable interest as well. To date, the dramatic improvement in design and fabrication of a molecular junction enables more precise measurements, but it also requests further investigation into the non-negligible contribution from the ionic transport in the solution, especially at room temperature. Recently, Doi *et al* reported on the transient electrical response of ions in the vicinity of biased electrodes.[123] Their results showed that ions rapidly responded to the strong fields near the electrode surface after turning on an applied voltage which screened the field in the process. Ions subsequently translocated in the weak electric field and slowly relaxed within the diffusion layer. The ionic current performed as a function of bias voltage and also as a function of ionic concentration (Fig. 2.5A). The interaction between the ions in the solution and the molecule in the junction has been highlighted in studies focusing on DNA molecules.[17,124–126] The interaction mainly consists of a binding between ions and molecules and a doping of ions into the space within the molecule, both of which are experimentally and theoretically studied to impact the charge

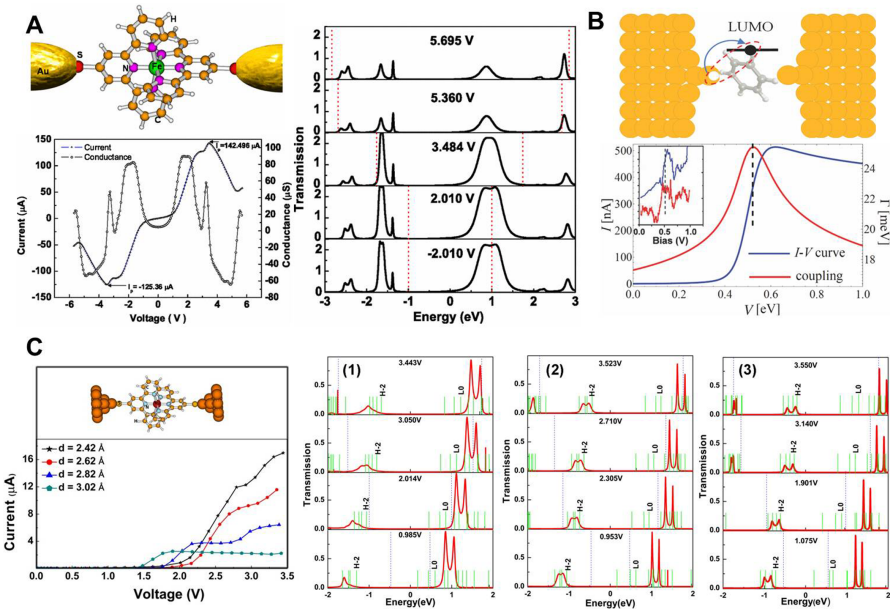

Figure 2.4: Bias-dependence electronic properties of molecular junctions. (A) top-left panel: schematic of the strongly coupled Fe-terpyridine-gold junction; bottom-left panel: calculated current and conductance as a function of applied bias; right panel: bias dependent transmission as a function of injection energy E. (B) top-panel: schematic of interface columb interaction; bottom panel: current (blue) and effective coupling Γ (red) as a function of the bias voltage for the interface Coulomb interaction. (C) left panel: calculated I-V characteristics for Rubis(terpyridine) molecular wires with different junction configurations (d refers to the interplanar distance between the sulfur and the nearest gold); right panel: bias dependent transmission as a function of injection energy for interfacial distances of (1) 2.42 Å, (2) 2.82 Å, and (3) 3.02 Å, respectively. (A) Reprinted from figure with permission from Pati R, McClain M, Bandyopadhyay A. *Phys Rev Lett.* 100, 246801, 2008. ©2008 American Physical Society.[118] (B) Reprinted with permission from Dubi Y. Dynamical coupling and negative differential resistance from interactions across the molecule-electrode interface in molecular junctions. *J Chem Phys.* 2013;139(15):154710. Copyright 2013 AIP Publishing LLC.[113] (C) Reprinted with permission from Dhungana KB, Mandal S, Pati R. Switching of conductance in a molecu lar wire: role of junction geometry, interfacial distance, and conformational change. *J Phys Chem C Nanomater Interfaces.* 2012;116(32): 1726817273. ©2012 American Chemical Society.[6]

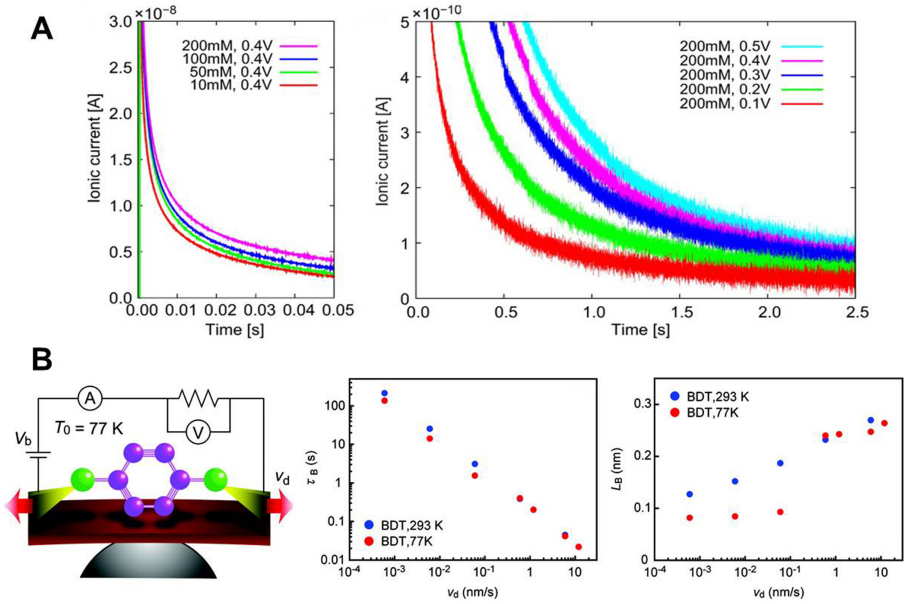

Figure 2.5: Environmental influence on molecular junction measurements with MCBJ approach. (A) Left panel: transient current response of NaCl solution under an applied potential of 0.4 V for several salt concentrations; right panel: current response for a concentration of 200 mM NaCl at various bias voltages. (B) Left panel: Schematic illustration of the experimental setup based on MCBJ at 77 K; junction lifetime τ_B vs junction stretching rate V_d (middle panel) and junction breakdown length L_B vs junction stretching rate V_d (right panel) for BDT single-molecule junction. Results acquired at 293 K are also shown for comparison. (A) Reprinted with permission from Doi K, Tsutsui M, Ohshiro T, et al. Nonequilibrium ionic response of biased mechanically controllable break junction (MCBJ) electrodes. *J Phys Chem C Nanomater Interfaces.* 2014;118(7):37583765. ©2014 American Chemical Society.[123] (B) Reprinted with permission from Tsutsui M, Taniguchi M, Kawai T. Atomistic mechanics and for mation mechanism of metal-molecule-metal junctions. *Nano Lett.* 2009;9(6):24332439. ©2009 American Chemical Society, reprinted with permission.[40]

transport process. Lowering the temperature to cryogenic levels greatly reduced the influence of thermal fluctuation on conductance, and in turn made the sensitivity to ionic influences more pronounced.

Temperature also has influences on the molecule-electrode junction. Measurements conducted at 77 K revealed the temperature dependence of a benzenedithiol junction life-time can be explained in terms of gold single-atom contact stability. This suggested that the

molecular junction lifetime at 77 K started to become shorter than the lifetime at room temperature under low strain rate conditions (Fig. 2.5B), where differences in the effects of thermal fluctuations on gold single-atom contact stability became notable.[40] Otherwise local heating, a common issue of current-carrying devices, is also observed for molecular junctions. A temperature increase by different degrees due to local heating was revealed for different molecular junctions. Electron-phonon scattering was suggested as the cause of local heating in MCBJs, which emerged at molecule-electrode interfaces and conse-quentially destabilized the junction.[78,127] Thus, severe electrical local heating has to be considered when discussing the resulting electronic properties.

2.8 Conclusion and Outlook

There is still plenty of room for improvement in the techniques involved in MCBJs. The following suggestions are just some of the potential issues that may be addressed in the near future.

1. It is now beneficial to incorporate other measurement techniques into multivariate corre-lation schemes alongside MCBJ conductance. This is already being done with Raman scattering,[28,29,41,128–130] but there is potential to use multivariate correlation to study mag-netic phenomenon such as the Kondo effect.[131,132] Optical manipulation of molecules in MCBJs is already a common practice,[57,58,133] however, further optical manipulation and measurement is also possible using Fourier transform IV and further UV/vis techniques.[47] Force is easily measured alongside conductance using conductance atomic force microscopy in much the same way SPMBJs are performed.[78,134] New methods for analyzing multivariate data sets are just now emerging, with great

potential for expansion and development.[8,23,26] *New coupled multivariate measurement techniques will have the ability to measure the behavior of MCBJs at finer resolutions, and retain the essential time-dependent nature of the evolving junction.*[27,70]

2. Water is an essential part in organic molecule junctions when the molecule must be kept in a natural solution. It has been simulated that water, along with ions in solution, may incorporate into DNA grooves and alter the available conductance channels.[135] However, the *effects of water on the conductance of complex molecules have not been studied thoroughly in laboratory experiments.*

3. Along the same line, electrochemical gating too can have a strong effect on the molecule. Specifically, theoretical investigations into electron transfer and *the effects of redox reactions on molecular orbital changes are beginning to show promise.*[112] The data analysis method of TVS provides very simplified models, but far more fundamental models are necessary.

4. Many of the organic molecules researchers study (DNA and proteins) are too large for traditional Hartree-Fock ab initio simulations. In order to fully understand these molecular junctions simulations are required, but often these simulations must be overly simplified. *Better simulation methods for large systems will be required in the future.*

5. For the development of far more stable junctions, it will become necessary to *utilize semiconductor electrodes which provide the potential for C-C and Si-C bonds at the molecule-electrode junction.*[35,136,137] This will also pave the way for more ad-vanced semiconducting molecular devices.[138]

6. It is also necessary to *develop stable dielectric and electrolytic media to stabilize molecular junctions* for use in future molecular electronics.[4]

In 1983, when Binnig and Rohrer were concluding the invention of the STM, they described the disadvantage of traditional tunnel junctions available at the time: once a metal-insulator-metal sandwich was manufactured, it was no longer possible to adjust the junction further.[34] The STM they developed solved this problem by using the vacuum barrier between the tip and substrate along with a piezoelectric transducer to allow easy adjust-ments to the junction. MCBJs are a natural extension of the desire to provide dynamic, easily modified mesoscopic junctions for fundamental physical studies. The STMs ability to scan the local density of states of the molecule is impressive, and when used as a probe to complete a single molecular circuit it becomes a fundamental tool for physicists and chemists to explore the fundamentals of their fields.

Chapter 3

Force and conductance molecular break junctions with time series crosscorrelation*

*J.M. Hamill, K. Wang, B. Xu. 2014. *Nanoscale* **6**:5657-5661. Reprinted here with permission of the publisher.

3.1 Abstract

Force and conductance, measured across 4,4'-bipyridine simultaneously, are crosscorrelated using a two dimensional (2D) histogram method. The result is a 2D multivariate statistical analysis superior to current one dimensional histogram techniques for exploring significant conductance and force modulations within SMBJs. This method is sensitive enough to cross-correlate signal modulations between force and conductance traces associated with contact geometry perturbations predicted in literature such as Au-molecule contact twisting and slipping during junction elongation.

3.2 Introduction

Nanoelectronic devices will incorporate science derived from single molecular break junctions, but only after the science of molecular-electrode contacts is better understood. Debate surrounds the mechanical and electrical properties of single molecular break junctions (SMBJs); and much of this concerns nonequilibrium contact geometry irregularities.[15,61,108,139–142] Fluctuations in the plateaus of SMBJs have been attributed to shot noise,[27] or 1/f noise,[2] but the dynamic nature of break junctions suggests close kinship between force and conductance in break junction measurements. Variable junction trajectories in SMBJs require researchers resort to statistical methods to determine expected values of molecular conductance and forces with standard deviation,[14] despite the observation that the statistics of SMBJs should be treated not as ensemble average measurements, but as time-dependent single molecular spectroscopy measurements.[70] Conductance 1D histograms (C-1DH) have been used to study SMBJs to determine most likely molecular conductances.[143] C-1DHs, however, provide limited understanding of the nature of SMBJs because larger trends overwhelm small details, even when displacement is accounted for in analysis.[7] Kirchhoff's superposition law results in a sum of the relatively large molecular conductance and the relatively small conductance

changes due to contact reorientation.[144] Often these small conductance perturbations are less than 0.1× the magnitude of the single molecular conductance. The central question in this letter is whether statistical techniques can distinguish significant contact modulations from background noise once the larger molecular conductance is removed. These techniques must preserve details of the time-dependent molecular spectroscopy, but still provide robustness and statistical confidence by averaging numerous individual traces of large data sets.

Time series analysis (TSA) has recently been adapted for SMBJs,[24,26] and for other force related molecular studies in the past few decades.[145,146] Autocorrelation, one TSA technique, was applied to SMBJ data creating a conductance two-dimensional autocorrelation histogram (C-2DACH) which revealed correlations between pairs of conductance values from the data set.[147] This is a powerful tool to discover information about the molecule and contact geometry in the break junction. It is suggested that this technique will be useful in investigating room temperature shot-noise.[27]

Autocorrelation is in a class of TSA devoted to single variable measurements, and is a single dimensional analysis. But it is a step towards multivariate TSA. The added dimension of a second variable, along with the TSA tools to analyze such data, provides insights into the nature of SMBJs.

Understanding of relationships between peaks in C-1DHs has improved with recent use of C-2DACH.[23] Binning force or conductance versus displacement traces into a 2D histogram grid (F-2DH or C-2DH) was also shown to be a useful tool to reveal details about the break point and final conductance in SMBJs.[7,9,23,105,148] This, especially when used in conjunction with the C-2DACH technique, was used in the past to determine a 4,4'-bipyridine (4,4'-bpy) molecule in a SMBJ can be oriented in one of two ways, each with a unique conductance value.[23] This phenomenon showed on a C-1DH as separate peaks and on a C-2DACH as an anticorrelated region at the intersection of the two conductances. Expanding the

C-2DACH to a multivariate force-conductance two-dimensional crosscorrelation histogram (FC-2DCCH) distinguishes characteristics of force traces which are statistically correlated with characteristics from conductance traces (and *vice versa*).

Herein, the C-2DACH technique is expanded to its multivariate equivalent, the FC-2DCCH, adding the second dimension of force to a powerful data analysis technique already being applied to conductance. The technique is then applied to a representative data set of about 100 conductance atomic force spectroscopy (C-AFM) SMBJ measurements of 4,4'-bpy (Fig. 3.1). This letter provides a proof-of-concept that the calculated correlated magnitudes of detailed modulations in force and conductance plateaus are comparable to *ab initio* investigations focused on trajectories of molecule-Au junctions reported in the literature.[7,11,89,105] This suggests that FC-2DCCH has the ability to discern miniature but significant fluctuations in force and conductance traces and allow deductions about sources and causes of those modulations.

3.3 Results and Discussion

A Au-4,4'-bpy-Au break junction, Fig. 3.1(d), was repeatedly created by approaching and retracting (at a rate of 40 nm s^{-1}) a Au coated AFM tip (with stiffness of 40 N m^{-1}) towards and away from 4,4'-bpy in toluene atop a Au(111) substrate. Labview programs read force and conductance [Fig. 3.1(b)]. A C-1DH [Fig. 3.1(c)], with bin size of 8.0×10^{-4} G_0, confirmed the most prominent conductance, corresponding to the first step in a sample trace when a single molecule was present in the junction, was at 8.65×10^{-3} G_0. This value is similar to previously published values.[3,149]

The saw tooth shape of the force traces yielded a poorly defined force 1D histogram (F-1DH). However, by subtracting removing the common slope, corresponding related to the constant rate of retraction of the cantilever, the saw tooth shape [Fig 3.1(b) curve 1] could be transformed into steps [Fig. 3.1(b) curve 2] which yielded a clearer histogram [Fig. 3.1(a)]

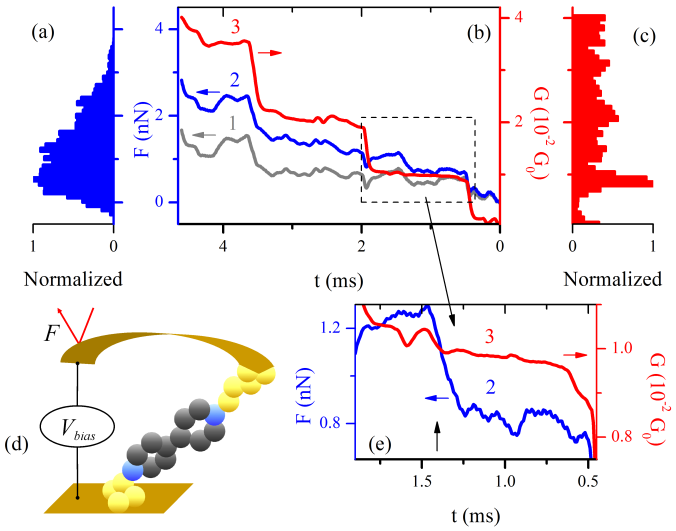

Figure 3.1: Example force (F) and conductance (G) traces with 1D histograms from about 30,000 data points. (a) Force 1D histogram from constant-slope-adjusted force traces; first peak at 0.68 nN; bin size is 0.087 nN. (b) Example force (1), constant-slope-adjusted force (2), and conductance (3) traces; thick lines over force traces depict slope of plateau before and after adjustment; square is expanded area in (e). (c) Conductance 1D histogram; first peak at 8.65×10^{-3} G_0; bin size is 8.0×10^{-4} G_0 (d) Schematic of experimental apparatus; force and conductance are measured as top electrode is retracted from bottom electrode while bias voltage is applied across 4,4-bipyridine. (e) Examples of the first plateau correlations of force (2) and conductance (3). Arrow illustrates example location of crosscorrelation.

using Eq. 3.1:

$$f_i^{new}\ [\mathrm{nN}] = f_i^{old}\ [\mathrm{nN}] - m\ [\mathrm{nN\ s^{-1}}]\ t_i\ [\mathrm{s}], \tag{3.1}$$

where $m = 40$ nN s^{-1}. This emphasized the flat force plateaus coinciding with the conductance plateaus, and had a negligible effect on the magnitude of step height change and modulations because these changes are abrupt and local. The prominent peak in Fig. 3.1(a) with bin size of 0.087 nN is at 0.68 nN, similar to published values.[9,12,13] Fig. 3.2(a) combined these two results in one force-conductance 2D histogram contour plot. The darker regions in Fig. 3.2(a) corresponded to the intersection of the most common conductance and force for each of the three plateaus. There is a dark region centered on a conductance of $8.65 \times 10^{-3}\ G_0$, and spanning across the force values associated with the first plateau of the break junction.

4,4'-bpy is exploited for SMBJs because of its rigid structure which orients itself vertically within Au-Au break junctions due to Au-H repulsion.[11] This orientation allows conductance to be measured longitudinally across the two benzene rings. Conductance modulations in phenyldithiolate never exceeded $1 \times 10^{-5}\ G_0$ in Hartree-Fock simulations,[150] suggesting that Au contacts will be the most likely source of conductance modulations, and not the aromatic rings of 4,4'-byp. As a consequence, the conductance modulations studied in this letter are expected to be due to adjustments occurring in the contacts as the junction progresses. Certain reorientations of 4,4'-bpy junctions will not be considered because the large changes involved are comparable to the changes involved when a molecule is removed from the junction entirely, and because they have been discussed elsewhere.[60]

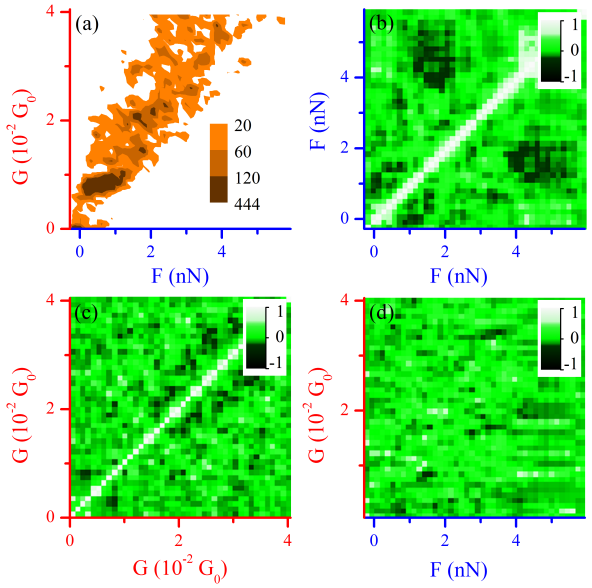

Figure 3.2: 2D histograms of force and conductance created from about 30,000 data points. (a) Force-conductance 2D histogram contour plot; dark region corresponds to the first plateau region. (b) Force 2D autocorrelation histogram; white is correlation of 1 and black is correlation of -1. (c) Conductance 2D autocorrelation histogram, intensity plot units same as (b). (d) Force-conductance 2D crosscorrelation histogram. Bin sizes are the same as those in Fig. 3.1.

3.3.1 Conductance autocorrelation

Autocorrelation H calculates the scaled covariance between two elements: 1) bin i of one trace histogram $g_i(l)$ compared with the mean $\langle g_i(l)\rangle_l$ of bin i from all the trace histograms and 2) bin j of the same sample $g_j(l)$ compared with the mean $\langle g_j(l)\rangle_l$ of bin j from all of the samples compares the scaled variance of a variable with itself, but itself offset using Eq. (3.2), where $\langle g_i(l)\rangle$ is the expected value of the counts g, in histogram bin i, as averaged over all the traces l, for the measured variable, conductance, and n is the number of bins i and j:[23]

$$H_g(i,j) = \frac{\langle [g_i(l) - \langle g_i(l)\rangle] * [g_j(l) - \langle g_j(l)\rangle]\rangle_l}{\sqrt{\langle [g_i(l) - \langle g_i(l)\rangle]^2\rangle_l \langle [g_j(l) - \langle g_j(l)\rangle]^2\rangle_l}}. \tag{3.2}$$

Usually autocorrelation takes a time-varying signal and offsets it in time, so that i and j represent moments in time where j is a time lagged behind (or before when the lag is negative) i, and then calculates the degree with which the signal and its offset are correlatedlinearly dependent. However, for this analysis, the histograms are being used instead of the signal, and therefore in this instance Fig. 3.2(c) i and j represent different binned units of conductance where j is lagged, or offset, from i by a certain amount of bins of conductance. The algorithm runs through all possible lags, from a lag of 0 G_0 when $i = j$, to a maximum lag determined by the bin with the largest value of conductance in the histograms. This is why the diagonal of Fig. 3.2(b) is 1: when the lag is 0 G_0, there is a perfect correlation between each histogram and itself. Qualitatively, Eq. (3.2) is the variances of the data in bin i or j, divided by a scaling factor that is the standard deviation which removes the units and normalizes the results. As stated previously, Eq. (3.2) is essentially a 1D analysis, in terms of the variable g. Eq. (3.2) was used to calculate Figs. 3.2(b) and 3.2(c), where the intensity plot ranges from -1 (anticorrelated) in black to 1 (correlated) in white. Autocorrelation is a useful tool in discovering repeating patterns in a single signal, or in a multiple samples of a single variable to determine if the signal is noise or information.

3.3.1.1 Example application of C-2DACH: DNA with Mg^{2+} ions and B-DNA vs. Z-DNA*

To better illustrate the application of the FC-2DCCH method which will be described in Section 3.3.3, included here is an experiment using the precursor C-2DACH method just described. The C-2DACH method is only concerned with the single variable of conductance, and thus is a single dimensional analysis, although it is plotted on a 2D intensity plot. However, here I will show that this method provides valuable information in its own right, and is a nice segue from techniques previously published to the new FC-2DCCH method I will present in Section 3.3.3. In this example, the method was applied to short stranded dsDNA data to help elucidate details from the C-1DHs which otherwise would have gone unnoticed. This experiment was not designed with the C-2DACH method in mind, and the the results of this analysis only served as a supplementary to clarify the behavior of the junction. Nonetheless, this only helps to illustrate the broad application of the analysis.

The various forms of dsDNA conformation can be accessed by altering the buffer surrounding the DNA.[21,151,152] One such example is the Z- form of DNA induced by increased cation concentration, Mg^{2+} being the easiest and most natural example. The goal of this experiment was to measure the difference in conductance between poly[d$(GC)_4$] in a solution which should retain the B- conformation of dsDNA, and the same sequence in various concentrations of Mg^{2+} ions which has the potential to shift the dsDNA to a Z-like conformation at concentrations above about 0.5 M Mg^{2+} based on previous studies. The actual transition to Z-DNA is highly dependent on the sequence and length of the dsDNA, and with any confidence we could not be certain that this full transition occurred, even at the highest tested concentration of 4.0 M Mg^{2+}. But previous studies on the causes of perturbation in

*The content of this section is derived from: K. Wang, J.M. Hamill, B. Xu. 2014. *Chemical Science* (Accepted Manuscript).

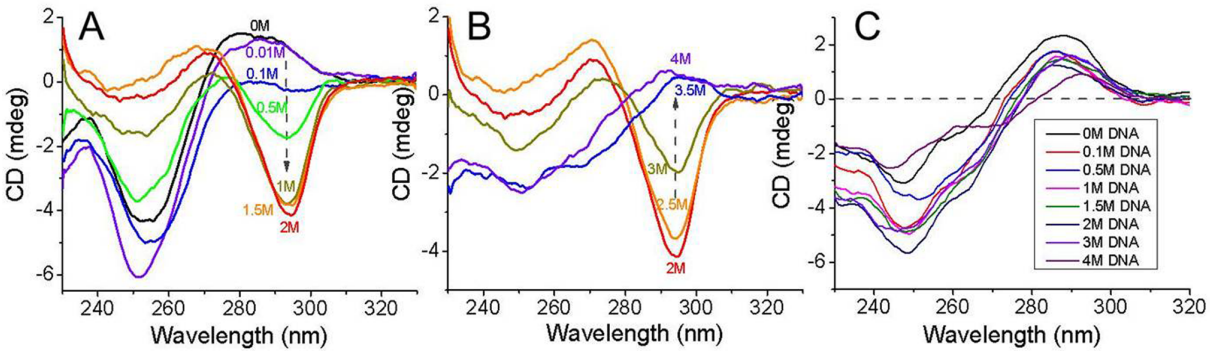

Figure 3.3: Circular dichroism measurements on poly[d(GC)$_4$] for incrementing concentrations of Mg^{2+}. At low concentrations CD curve resembles B-DNA;[21,154,155] the progression from 0.0 M to 2.0 M resembles the transition from B-DNA to Z-DNA; high concentrations, 3.0 M and 4.0 M, deviate from Z-DNA but possibly resemble λ-DNA indicating considerable aggregation.[18,156–158] Aggregation of ion confuses CD measurements, but has little effect on SPM conductance measurements due to the nature of the Au-molecule-Au junction.

B-DNA conformation gave us confidence that the dsDNA was altered significantly nonetheless.[17,20,135,153] This prediction was confirmed by the circular dichroism measurements in Fig. 3.3 which showed clear conformation change.

Using SPM SMBJs we measured the conductance of the dsDNA at incrementing concentrations of Mg^{2+}: 0.0 M, 0.1 M, 0.5 M, 1.0 M, 1.5 M, 2.0 M, 3.0 M, and 4.0 M. At low concentrations of Mg^{2+} the primary peak in the C-1DHs was at 1.03×10^{-3} G_0 (Fig. 3.4B), and we associated this to B-DNA because this conductance had been previously measured for similar sequences.[64,135] The primary peak was always accompanied with a second peak at about twice the conductance of the primary peak corresponding to junctions with two molecules in the junction. As the concentration of Mg^{2+} increased, these peaks did not move position, but shrank in height and overall area. At a Mg^{2+} concentration of 0.5 M and more so until 4.0 M (Fig. 3.4A) a second pair of peaks became obvious at a value of 2.79×10^{-5} G_0.

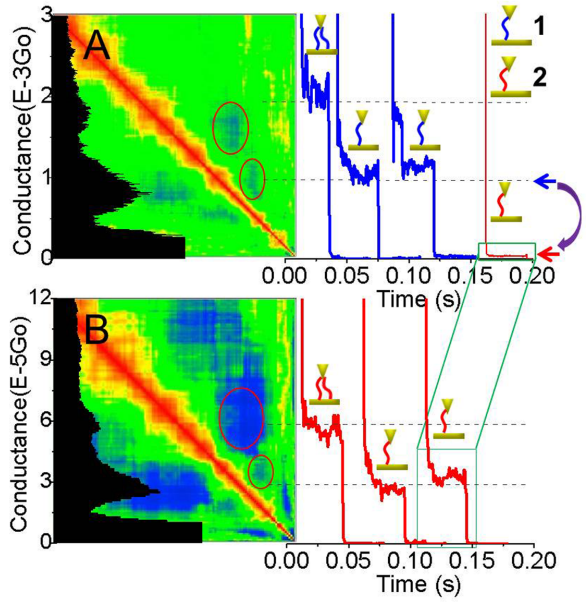

Figure 3.4: Conductance measurements on the scales (A)$\approx 1\times10^{-5}\ G_0$ and (B)$\approx 1\times10^{-3}\ G_0$ for dsDNA in 1.0 M Mg^{2+}. The profile of C-1DHs for each concentration of Mg^{2+} are nearly indistinguishable: only the relative height and area varies as depicted in Fig. 3.5. Intensity plots are C-2DACHs for both concentrations. Anticorrelated (blue) regions are seen at the intersection of the first and second peaks of the C-1DHs.

As the Mg^{2+} concentration increased, the height and area of these peaks increased, but they did not change location. These could be tentatively associated with a Z-like conformation of dsDNA.

Unfortunately, the conductance of these separate pairs of peaks did not make it possible to measure them together in the same trace. However, by creating C-1DHs from equal numbers of traces, the areas of the primary peaks in each pair could be compared using Eq. 3.3:

$$TD_{SPM} = A_Z/(A_Z + A_B). \tag{3.3}$$

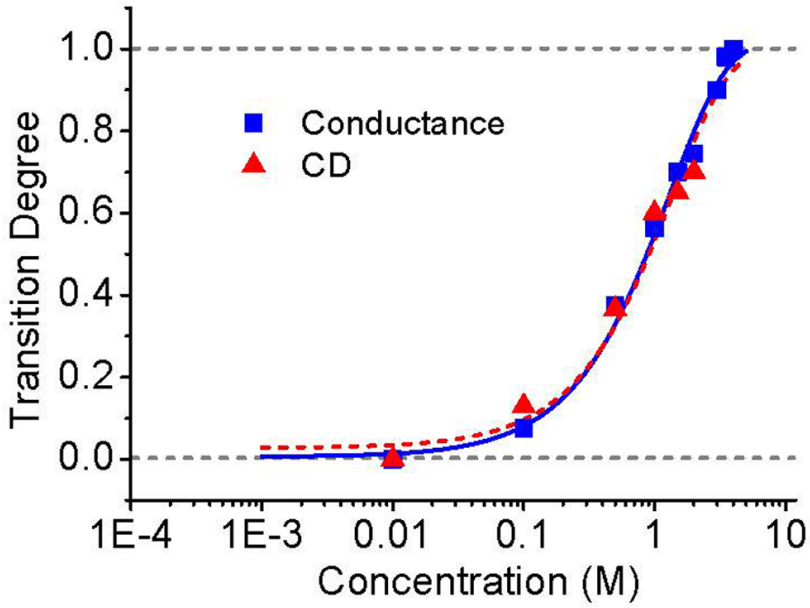

Figure 3.5: B-Z DNA transition plot using SPM conductance measurements and Eq. 3.3 in blue, and CD measurements in red.

We showed (Fig. 3.5) that the manner at which the B-DNA decreased in frequency while the Z-like form increased followed the pattern measured in the CD, which is the traditionally accepted tool to measure this transition.

So our interpretation of the data was that in each junction the DNA measured was either B-DNA or Z-like DNA, and nothing in between. One possible way for this to occur is for each junction to involve only a single molecule, or two similar conformed molecules. We employed the C-2DACH to help verify this hypothesis. The anticorrelation regions in Fig. 3.4 show that, statistically, each junction either involved only one or two molecules, but never two molecules breaking to one. This information would have been impossible to derive from the C-1DHs alone, and could only be spoken of in qualitative terms from subjective observations made by comparing in person all of the conductance traces. Instead, quantitative values can

be assigned to the degree at which the physical phenomenon occurs in the data. This is the value of the C-2DACH in its broad application. A more detailed discussion of this algorithm is included in Appendix A.

3.3.2 Correlation

Eq. (3.4) calculates correlation ρ of two variables without a time lag, where

$$\rho_{f,g}(i) = \frac{\langle [f_i(l) - \langle f_i(l) \rangle] * [g_i(l) - \langle g_i(l) \rangle] \rangle_l}{\sqrt{\langle [f_i(l) - \langle f_i(l) \rangle]^2 \rangle_l \langle [g_i(l) - \langle g_i(l) \rangle]^2 \rangle_l}}. \tag{3.4}$$

Bin i of variable f was only compared with bin i of variable g. Because there is no offset, it is not beneficial to plot this in a 2D grid, although this is now a 2D analysis. Correlation calculates how much two variables depend upon one another at each point.

3.3.3 Force and conductance crosscorrelation

Finally, crosscorrelation r reintroduces the time lag from autocorrelation into the correlation calculation for two variables using Eq. (3.5):

$$r_{f,g}(i,j) = \frac{\langle [f_i(l) - \langle f_i(l) \rangle] * [g_j(l) - \langle g_j(l) \rangle] \rangle_l}{\sqrt{\langle [f_i(l) - \langle f_i(l) \rangle]^2 \rangle_l \langle [g_j(l) - \langle g_j(l) \rangle]^2 \rangle_l}}. \tag{3.5}$$

In other words, autocorrelation is the special case when a variable is crosscorrelated with itself, and correlation is the special case when $i = j$ for two variables. For Fig. 3.2(d), the conductance array was substituted for one of the arrays in the force calculation to result in a FC-2DCCH. Because each sample pair is parameterized by time, direct comparisons between the force and conductance within that pair were permissible. The result is a calculation for the correlation (anticorrelation) between a measured value of conductance and a measured

value of force. Specifically, this is a crosscorrelation calculation between two variables with the second variable offset by incrementing lag as with autocorrelation. Correlated regions are found at the loci of the conductance and force values associated with each of the plateaus.

Two dimensional autocorrelation histograms for both force (F-2DACH) and conductance and force (F-2DACH) were created [Figs. 3.2(b) and 3.2(c)]. This involved a calculation of autocorrelation in which multiple samples of a single variable were binned individually, and each histogram was autocorrelated against the average of the histograms of the whole data set, resulting in a calculation of which values of the variable occurred together, on average, in individual traces. Noticeable features in Fig. 3.2(b) were the bands of anticorrelation parallel to the center diagonal of width 0.7 nN. This was the average separation between adjacent force plateaus in the constant-slope adjusted-force traces. A similar feature was observed in Fig. 3.2(c) in which a separation of about 0.01 G_0 was the average.

It is standard procedure in TSA to remove global trends in the data in order to observe behavior on smaller time scales. To this end, Labview subroutines parsed the segment of each force and conductance pair where the conductance trace entered and left a window around 8.65×10^{-3} G_0. This removed the larger trend related to the decreasing number of molecules in the junction. These segments were then checked to ensure they were of minimum length to exclude any conductance samples which did not have a plateau in that window. Fig. 3.1(e) shows an example pair of traces clipped down to the first plateau where close relationships between modulations in force and conductance are observed. Finally, the mean of each trace, both force and conductance, were subtracted to offset each trace to zero. This ensured that when the correlation calculations were conducted, only the force changes ΔF and conductance changes ΔG, measured from the plateau, were compared and not global trends encompassing the entire plateau. These were the segments which were used to create the plots in Fig. 3.6.

ΔF and ΔG 2DHs [Figs. 3.6(a), 3.6(c), and 3.6(e)] were created to emphasize the distribution of values. Bin sizes were 0.077 ms for time, 0.020 nN for force, and 1.4×10^{-4} G_0 for conductance. Fig. 3.6(c) revealed no significant trend in ΔG aside from the Gaussian distribution. Fig. 3.6(a), however, showed a tendency towards a multi-modal behavior in ΔF, an attribute also reflected in the FC-2DH of Fig. 3.6(e). This multi-modal distribution of ΔF suggested it favored specific magnitudes of change. This is further clarified in the F-2DACH [Fig. 3.6(b)] and G-2DACH [Fig. 3.6(d)]. In Fig. 3.6(b) the change in force of -0.21 nN was correlated to a change in force of 0.29 nN. Similarly, in Fig. 3.6(d), a ΔG of -3.8×10^{-5} G_0 was anti-correlated to a ΔG of -1.5×10^{-3} G_0. In both cases, this change was from the average plateau value. The sign not only revealed significant correlations in the changes, but it specified whether those changes result in an increase or a decrease in conductance and force. The correlation (anticorrelation) of pairs of force (conductance) values indicated that within any given trace, there was a strong possibility that when a change of ΔF (ΔG) of one value was observed, so too was the ΔF (ΔG) of the other. Fig. 3.6(f) indicated that there was a correlation, for example, between a decrease in force of 0.21 nN and an increase in conductance of 5.0×10^{-4} G_0; but Fig. 3.6(f) also indicated a correlation between a decrease in force of 0.1 nN and a decrease in conductance of 1.0×10^{-3} G_0.

The black circle in Fig. 3.6(f) highlighted the correlated region at the location $(\Delta F, \Delta G)$ $= (0.1 \text{ nN}, 6.0 \times 10^{-4}\ G_0)$. When a molecule twisted during the initial stages of a break junction there was a corresponding effect on the conductance and force.[7,105,159] During the relaxation of the twist, when bond distances between the conducting $\pi-$orbital of the molecule and the $s-$orbital of the Au were slowly returning to an overlapped orientation, there were periods of rapid change. One such jump resulted in a rise and fall of force of magnitude 0.08 nN and corresponding increase in conductance of 6×10^{-5} G_0. High conductance could be achieved either when the molecule was in a perpendicular orientation within the junction and the N-Au bond was minimized, or when the molecule was orientated

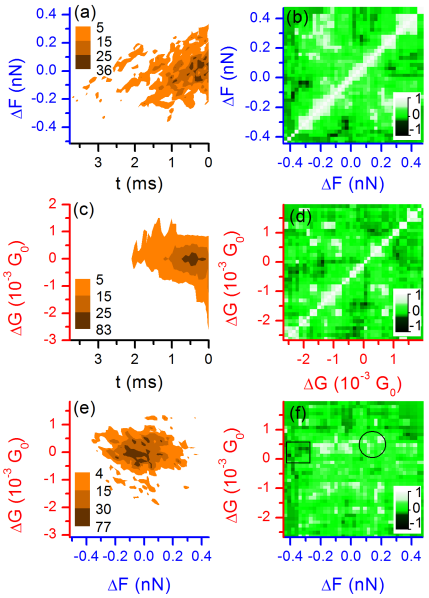

Figure 3.6: Histograms for traces clipped to the first plateau from about 10,000 data points. a) Force 2D histogram. b) Force 2D autocorrelation histogram. c) Conductance 2D histogram. d) Conductance 2D autocorrelation histogram. e) Force-conductance 2D histogram. f) Force-conductance 2D crosscorrelation histogram; square and circle highlight (anti)correlated regions. Time bin size is 0.077 ms; force bin size is 0.020 nN; conductance bin size is 1.4×10^{-4} G_0.

at a close angle to the substrate, allowing the π^*-LUMO to be more favorably aligned with the s-orbital of the Au. These competing influences on the conductance of the 4,4'-bpy break junction made the conductance highly sensitive to the orientation of the molecule and the contacts, resulting in modulations of the conductance and force when any of these factors changed during elongation. The DFT simulation calculated the predicted changes in force and conductance due to specific orientation changes, and the FC-2DCCH results suggested promising agreement with the predictions, within a reasonable order of magnitude and limitations of the uncertainties as a consequence of discrete bin sizes and resolution.

The second region of interest, marked with a black square in Fig. 3.6(f), corresponded to $(\Delta F, \Delta G) = (-0.40 \text{ nN}, 1.2 \times 10^{-4}\ G_0)$. This pair was similar to the area marked with an arrow in Fig. 1(e). A nitrogen terminated molecule bonding initially to the second tier of the Au contact, before slipping down to the apex under strain, showed similar characteristics in the force and conductance traces.[11] During this slip the force quickly changed by -0.6 nN and a rise and fall of conductance of magnitude $4 \times 10^{-4}\ G_0$ was calculated.[7] Within an order of magnitude, the simulated results of this precise junction trajectory, and the FC-2DCCH, as calculated from experimental data here, are in agreement.

Au-Au chains formed at the contacts in a 4,4'-bpy SMBJ were predicted to undergo both conductance increase and decrease as the bond angles of the zigzag chain adjusted during junction elongation.[89] Oscillations in the conductance of about 20% due to Peierl's distortion were reported when the number of Au atoms in a chain went from odd to even. Au chains as long as four Au atoms were possible when involved in a SMBJ,[13] so these oscillations occur more than once as more Au atoms are added to the chain in a single plateau, prior to rupture. Other studies suggested large force changes do not necessarily result in large conductance changes.[10] Various other possible Au junction trajectories have been considered with consequences for the correlated force and conductance modulation.[11,25,81]

3.4 Conclusion

We have shown the FC-2DCCH technique provides the experimentalist with tools not yet available to plumb molecular-electrode interfaces in nonequilibrium junctions. Higher resolution samples of Au-Au junctions will allow for smaller bin sizes and may reveal the types of conductance oscillations referred to in the previous paragraph. Furthermore, dynamic behavior within molecules will also be measurable. Simulation on the unfolding of a molecule shows promising correlation between a force change of 0.044 nN and changes in the transmission function of the molecular junction.[160] Other possibilities might include quantum chemistry calculations predicting isomers with transition energies less than 1eV can be measured with CM-AFM to experimentally establish the transition force and identify the effects this transition has on the orbitals and conductance. Such low transition energies might be associated with a ruptured hydrogen bond, or the disruption of a van der Waal's interaction. Short polymers seem a likely candidate.

In conclusion, by expanding upon recent developments in SMBJ data analysis techniques, and drawing upon established formulations in TSA, a 2D crosscorrelation analysis approach is presented with the ability to allow experiments to compare results to predictions made by first principle simulations for fields including quantum chemistry, molecular force spectroscopy, and molecular electronics. Force and conductance, when measured in unison, were crosscorrelated to compare correlations between modulations of each. Specific changes within conductance plateaus were correlated to modulations within the corresponding force trace, and the magnitude of these modulations found good agreement with break junction trajectories predicted using ab initio calculations. This suggested the capacity for TSA to discover many of the subtleties of single molecular conductance still hiding in the data and allow for closer cooperation between experiments and simulations.

Chapter 4

Conclusion

4.1 A Review of the past with an eye on the future

The method presented here offers immense flexibility. Two time-dependent variables, measured concurrently, can be crosscorrelated using this algorithm. The dependency of single molecular conductance on numerous factors suggests that a better understanding of SMBJs can be achieved by developing imaginative ways to measure these variables alongside conductance. Ch. 2 explores this in some detail, after it first reviews the current state-of-the-art of SPM SMBJs. Optical correlation is already showing promise, but more dependencies should be considered.

4.2 An Experiment with future potential

While 4,4'-bpy has proven time and again to be a valuable test bed for SMBJs, the analysis presented in Ch. 3, though a good start, provides only limited insight. This is mainly due to the limited degrees of freedom provided by the 4,4'-bpy molecule. What is needed is a molecule which can be perturbed between multiple states by small manipulations of force.

If such a molecule were used in the FC-2DCCH analysis, it may be possible to distinguish the conductance of each state by correlating these states with the force necessary to achieve the state.

4.3 Final thoughts

The time-dependence of the current algorithm is removed early on in the calculation. A more robust algorithm must be developed for true time-dependence to be apart of this analysis. There is a library of methods available in the discipline of time-series analysis, and it is a matter of simply choosing the most appropriate. Current publications are numerous on the topic of multifractal stochastic nonlinear time-series in physical journals, mainly used to study chaotic systems. This is evidence that the methods are being developed for physical systems.

Bibliography

[1] M. A. Reed, C. Zhou, C. J. Muller, T. P. Burgin, and J. M. Tour, Science **278**, 252 (1997).

[2] N. Tao, Nature Nanotechnology **1**, 173 (2006).

[3] B. Xu and N. J. Tao, Science **301**, 1221 (2003).

[4] S. Lindsay, Faraday Discuss. **131**, 403 (2006).

[5] S. M. Lindsay and M. A. Ratner, Adv Mater **19**, 23 (2007).

[6] K. B. Dhungana, S. Mandal, and R. Pati, J Phys Chem C **116**, 17268 (2012).

[7] M. Kamenetska, M. Koentopp, A. C. Whalley, Y. S. Park, M. L. Steigerwald, C. Nuckolls, M. S. Hybertsen, and L. Venkataraman, Phys. Rev. Lett. **102**, 126803(01) (2009).

[8] M. Frei, S. V. Aradhya, M. S. Hybertsen, and L. Venkataraman, J. Am. Chem. Soc. **134**, 4003 (2012).

[9] M. Frei, S. V. Aradhya, M. Koentopp, M. S. Hybertsen, and L. Venkataraman, Nano Lett. **11**, 1518 (2011).

[10] Á. J. Pérez-Jiménez, J. Phys. Chem. B **109**, 10052 (2005).

[11] A. J. Pérez-Jiménez, J. C. Sancho-García, and J. M. Pérez-Jordá, J. Chem. Phys. **123**, 134309 (2005).

[12] R. Stadler, K. S. Thygesen, and K. W. Jacobsen, Phys Rev B **72**, 241401 (2005).

[13] P. Vélez, S. A. Dassie, and E. P. M. Leiva, Phys Rev B **81**, 235435 (2010).

[14] B. Xu, X. Xiao, and N. J. Tao, J. Am. Chem. Soc. **125**, 16164 (2003).

[15] J. Zhou and B. Xu, Appl. Phys. Lett. **99**, 042104 (2011).

[16] R. E. Dickerson, H. R. Drew, B. N. Conner, R. M. Wing, A. V. Fratini, and M. L. Kopka, Science **216**, pp.475 (1982).

[17] J. C. Genereux and J. K. Barton, Chem. Rev. **110**, 1642 (2010).

[18] E. Hamori and T. M. Jovin, Biophys. Chem. **26**, 375 (1987).

[19] T. M. Jovin, D. M. Soumpasis, and L. P. McIntosh, Annu. Rev. Phys. Chem. **38**, 521 (1987).

[20] S. S. Mallajosyula, A. Gupta, and S. K. Pati, J. Phys. Chem. A **113**, 3955 (2009).

[21] F. M. Pohl and T. M. Jovin, J. Mol. Biol. **67**, 375 (1972).

[22] C. R. Treadway, M. G. Hill, and J. K. Barton, Chem. Phys. **281**, 409 (2002).

[23] P. Makk, D. Tomaszewski, J. Martinek, Z. Balogh, S. Csonka, M. Wawrzyniak, M. Frei, L. Venkataraman, and A. Halbritter, ACS Nano **6**, 3411 (2012).

[24] C. Nef, P. L. T. M. Frederix, J. Brunner, C. Schönenberger, and M. Calame, Nanotechnology **23**, 365201 (2012).

[25] M. J. Lagos, P. A. S. Autreto, D. S. Galvao, and D. Ugarte, J. Appl. Phys. **111**, 124316 (2012).

[26] S. V. Aradhya, M. Frei, A. Halbritter, and L. Venkataraman, ACS Nano **7**, 3706 (2013).

[27] D. Natelson, ACS Nano **6**, 2871 (2012).

[28] T.-H. Park and M. Galperin, Europhys. Lett. **95**, 27001 (2011).

[29] D. R. Ward, N. J. Halas, J. W. Ciszek, J. M. Tour, Y. Wu, P. Nordlander, and D. Natelson, Nano Lett. **8**, 919 (2008).

[30] R. P. Feynman, Engineering and Science **23**, 22 (1960).

[31] A. von Hippel, Science **123**, 315 (1956).

[32] G. E. Moore, Electronics Magazine pp. 114–117 (1965).

[33] A. Aviram and M. Ratner, Chem. Phys. Lett. **29**, 277 (1974).

[34] G. Binnig and H. Rohrer, Surf. Sci. **126**, 236 (1983).

[35] N. P. Guisinger, N. L. Yoder, and M. C. Hersam, Proc. Natl. Acad. Sci. U. S. A. **102**, 8838 (2005).

[36] M. Taniguchi, M. Tsutsui, R. Mogi, T. Sugawara, Y. Tsuji, K. Yoshizawa, and T. Kawai, J. Am. Chem. Soc. **133**, 11426 (2011).

[37] M. Tsutsui, M. Taniguchi, and T. Kawai, J. Am. Chem. Soc. **131**, 10552 (2009).

[38] M. Elbing, R. Ochs, M. Koentopp, M. Fischer, C. von Hanisch, F. Weigend, F. Evers, H. B. Weber, and M. Mayor, Proc. Natl. Acad. Sci. U. S. A. **102**, 8815 (2005).

[39] J. Reichert, H. B. Weber, M. Mayor, and H. von Lohneysen, Appl. Phys. Lett. **82**, 4137 (2003).

[40] M. Tsutsui, M. Taniguchi, and T. Kawai, Nano Lett. **9**, 2433 (2009).

[41] D. Natelson, Y. Li, and J. B. Herzog, Phys. Chem. Chem. Phys. **15**, 5262 (2013).

[42] K. Slowinski, R. V. Chamberlain, C. J. Miller, and M. Majda, J. Am. Chem. Soc. **119**, 11910 (1997).

[43] S. Gregory, Phys. Rev. Lett. **64**, 689 (1990).

[44] J. Chen, M. A. Reed, A. M. Rawlett, and J. M. Tour, Science **286**, 1550 (1999).

[45] C. Zhou, M. R. Deshpande, M. Reed, L. Jones, and J. Tour, Appl. Phys. Lett. **71**, 611 (1997).

[46] C. M. Fischer, M. Burghard, S. Roth, and K. V. Klitzing, Appl. Phys. Lett. **66**, 3331 (1995).

[47] R. L. McCreery and A. J. Bergren, Adv Mater **21**, 4303 (2009).

[48] Z. Zhong, D. Wang, Y. Cui, M. W. Bockrath, and C. M. Lieber, Science **302**, 1377 (2003).

[49] J. G. Kushmerick, D. B. Holt, S. K. Pollack, M. A. Ratner, J. C. Yang, T. L. Schull, J. Naciri, M. H. Moore, and R. Shashidhar, J. Am. Chem. Soc. **124**, 10654 (2002).

[50] L. A. Bumm, J. J. Arnold, M. T. Cygan, T. D. Dunbar, T. P. Burgin, L. J. II, D. L. Allara, J. M. Tour, and P. S. Weiss, Science **271**, pp.1705 (1996).

[51] D. J. Wold and C. D. Frisbie, J. Am. Chem. Soc. **123**, 5549 (2001).

[52] X. D. Cui, A. Primak, X. Zarate, J. Tomfohr, O. F. Sankey, A. L. Moore, T. A. Moore, D. Gust, L. A. Nagahara, and S. M. Lindsay, J. Phys. Chem. B **106**, 8609 (2002).

[53] M. Dorogi, J. Gomez, R. Osifchin, R. P. Andres, and R. Reifenberger, Phys Rev B **52**, 9071 (1995).

[54] O. Y. Kolesnychenko, O. I. Shklyarevskii, and H. van Kempen, Rev. Sci. Instrum. **70**, 1442 (1999).

[55] C. J. Muller, J. M. Krans, T. N. Todorov, and M. A. Reed, Phys Rev B **53**, 1022 (1996).

[56] D. Dulić, S. J. van der Molen, T. Kudernac, H. Jonkman, J. De Jong, T. Bowden, J. Van Esch, B. Feringa, and B. Van Wees, Phys. Rev. Lett. **91**, 207402 (2003).

[57] J. He, F. Chen, P. A. Liddell, J. Andrasson, S. D. Straight, D. Gust, T. A. Moore, A. L. Moore, J. Li, O. F. Sankey, and S. M. Lindsay, Nanotechnology **16**, 695 (2005).

[58] Y. Kim, T. J. Hellmuth, D. Sysoiev, F. Pauly, T. Pietsch, J. Wolf, A. Erbe, T. Huhn, U. Groth, U. E. Steiner, and E. Scheer, Nano Lett. **12**, 3736 (2012).

[59] R. Landauer, IBM Journal of Research and Development **1**, 223 (1957).

[60] S. V. Aradhya, M. Frei, M. S. Hybertsen, and L. Venkataraman, Nat. Mater. pp. 872–876 (2012).

[61] R. A. Wassel, R. R. Fuierer, N. Kim, and C. B. Gorman, Nano Lett. **3**, 1617 (2003).

[62] M. T. González, S. Wu, R. Huber, S. J. van der Molen, C. Schönenberger, and M. Calame, Nano Lett. **6**, 2238 (2006).

[63] M. Mayor and H. B. Weber, Angew. Chem., Int. Ed. **43**, 2882 (2004).

[64] B. Xu, P. Zhang, X. Li, and N. Tao, Nano Lett. **4**, 1105 (2004).

[65] E. Braun, Y. Eichen, U. Sivan, and G. Ben-Yoseph, Nature **391**, 775 (1998).

[66] D. Porath, A. Bezryadin, S. De Vries, and C. Dekker, Nature **403**, 635 (2000).

[67] H.-W. Fink and C. Schönenberger, Nature **398**, 407 (1999).

[68] Y. Okahata, T. Kobayashi, K. Tanaka, and M. Shimomura, J. Am. Chem. Soc. **120**, 6165 (1998).

[69] A. Y. Kasumov, M. Kociak, S. Gueron, B. Reulet, V. Volkov, D. Klinov, and H. Bouchiat, Science **291**, 280 (2001).

[70] A. Nitzan and M. A. Ratner, Science **300**, 1384 (2003).

[71] J. He, O. Sankey, M. Lee, N. Tao, X. Li, and S. Lindsay, Faraday Discuss. **131**, 145 (2006).

[72] J. Tomfohr and O. F. Sankey, J. Chem. Phys. **120**, 1542 (2004).

[73] X. Cui, A. Primak, X. Zarate, J. Tomfohr, O. Sankey, A. Moore, T. Moore, D. Gust, G. Harris, and S. Lindsay, Science **294**, 571 (2001).

[74] W. Haiss, R. J. Nichols, H. van Zalinge, S. J. Higgins, D. Bethell, and D. J. Schiffrin, Phys. Chem. Chem. Phys. **6**, 4330 (2004).

[75] J. G. Kushmerick, Materials Today pp. 26–30 (2005).

[76] A. Salomon, D. Cahen, S. Lindsay, J. Tomfohr, V. Engelkes, and C. Frisbie, Adv Mater **15**, 1881 (2003).

[77] K. Yoshizawa, Acc. Chem. Res. **45**, 1612 (2012).

[78] Z. Huang, B. Xu, Y. Chen, M. D. Ventra, and N. Tao, Nano Lett. **6**, 1240 (2006).

[79] Y.-C. Chen and M. Di Ventra, Phys. Rev. Lett. **95**, 166802 (2005).

[80] D. Segal and A. Nitzan, J. Chem. Phys. **117**, 3915 (2002).

[81] P. E. Marszalek, W. J. Greenleaf, H. Li, A. F. Oberhauser, and J. M. Fernandez, Proc. Natl. Acad. Sci. U. S. A. **97**, 6282 (2000).

[82] M. Büttiker, Y. Imry, R. Landauer, and S. Pinhas, Phys Rev B **31**, 6207 (1985).

[83] Y. Dubi, J. Chem. Phys. **138**, 114706 (2013).

[84] B. Xu, X. Xiao, X. Yang, L. Zang, and N. Tao, J. Am. Chem. Soc. **127**, 2386 (2005).

[85] W. Hong, D. Z. Manrique, P. Moreno-Garcia, M. Gulcur, A. Mishchenko, C. J. Lambert, M. R. Bryce, and T. Wandlowski, J. Am. Chem. Soc. **134**, 2292 (2012).

[86] G.-P. Zhang, G.-C. Hu, Y. Song, Z.-L. Li, and C.-K. Wang, J Phys Chem C **116**, 22009 (2012).

[87] M. J. Lagos, F. Sato, D. S. Galvão, and D. Ugarte, Phys. Rev. Lett. **106**, 055501 (2011).

[88] V. Rodrigues and D. Ugarte, Phys Rev B **63**, 073405 (2001).

[89] F. Tavazza, S. Barzilai, D. T. Smith, and L. E. Levine, J. Appl. Phys. **113**, 054316 (2013).

[90] A. Thiess, Y. Mokrousov, S. Blügel, and S. Heinze, Nano Lett. **8**, 2144 (2008).

[91] M. del Valle, R. Gutiérrez, C. Tejedor, and G. Cuniberti, Nature Nanotechnology **2**, 176 (2007).

[92] C. Zhang, Y. He, H.-P. Cheng, Y. Xue, M. A. Ratner, X.-G. Zhang, and P. Krstic, Phys Rev B **73**, 125445 (2006).

[93] M. Tsutsui and M. Taniguchi, Sensors **12**, 7259 (2012).

[94] F. Chen, C. Nuckolls, and S. Lindsay, Chem. Phys. **324**, 236 (2006).

[95] D. I. Gittins, D. Bethell, D. J. Schiffrin, and R. J. Nichols, Nature **408**, 67 (2000).

[96] W. Haiss, H. van Zalinge, S. J. Higgins, D. Bethell, H. Hbenreich, D. J. Schiffrin, and R. J. Nichols, J. Am. Chem. Soc. **125**, 15294 (2003).

[97] N. J. Tao, Phys. Rev. Lett. **76**, 4066 (1996).

[98] B. Xu, H. He, and N. J. Tao, J. Am. Chem. Soc. **124**, 13568 (2002).

[99] Z.-L. Li, B. Zou, C.-K. Wang, and Y. Luo, Phys Rev B **73**, 075326 (2006).

[100] X. Xiao, L. A. Nagahara, A. M. Rawlett, and N. Tao, J. Am. Chem. Soc. **127**, 9235 (2005).

[101] F. Chen, J. He, C. Nuckolls, T. Roberts, J. E. Klare, and S. Lindsay, Nano Lett. **5**, 503 (2005).

[102] X. Xiao, D. Brune, J. He, S. Lindsay, C. B. Gorman, and N. Tao, Chem. Phys. **326**, 138 (2006).

[103] J. Beebe, B. Kim, J. Gadzuk, C. Daniel Frisbie, and J. Kushmerick, Phys. Rev. Lett. **97**, 026801 (2006).

[104] I. Bâldea, Nanoscale **5**, 9222 (2013).

[105] S. Y. Quek, M. Kamenetska, M. L. Steigerwald, H. J. Choi, S. G. Louie, M. S. Hybertsen, J. B. Neaton, and L. Venkataraman, Nature Nanotechnology **4**, 230 (2009).

[106] H. Song, Y. Kim, Y. H. Jang, H. Jeong, M. A. Reed, and T. Lee, Nature **462**, 1039 (2009).

[107] S. Ho Choi, B. Kim, and C. D. Frisbie, Science **320**, 1482 (2008).

[108] S. Guo, J. Hihath, I. Díez-Pérez, and N. Tao, J. Am. Chem. Soc. **133**, 19189 (2011).

[109] P.-W. Chiu and S. Roth, Appl. Phys. Lett. **92**, 042107 (2008).

[110] M. C. Lennartz, N. Atodiresei, V. Caciuc, and S. Karthäuser, J Phys Chem C **115**, 15025 (2011).

[111] J. M. Artés, M. López-Martínez, A. Giraudet, I. Díez-Pérez, F. Sanz, and P. Gorostiza, J. Am. Chem. Soc. **134**, 20218 (2012).

[112] I. Bâldea, J Phys Chem C **117**, 25798 (2013).

[113] Y. Dubi, J. Chem. Phys. **139**, 154710 (2013).

[114] I. Díez-Pérez, J. Hihath, Y. Lee, L. Yu, L. Adamska, M. A. Kozhushner, I. I. Oleynik, and N. Tao, Nature Chemistry **1**, 635 (2009).

[115] A. Saraiva-Souza, F. M. de Souza, V. F. P. Aleixo, E. C. Girao, J. M. Filho, V. Meunier, B. G. Sumpter, A. G. S. Filho, and J. Del Nero, J. Chem. Phys. **129**, 204701 (2008).

[116] X. Zhao, J. Li, T. C. Au Yeung, C. H. Kam, Q.-H. Chen, and C. Q. Sun, J. Appl. Phys. **107**, 094312 (2010).

[117] Y. Tsuji and K. Yoshizawa, J Phys Chem C **116**, 26625 (2012).

[118] R. Pati, M. McClain, and A. Bandyopadhyay, Phys. Rev. Lett. **100**, 246801(01) (2008).

[119] M. Bürkle, J. K. Viljas, D. Vonlanthen, A. Mishchenko, G. Schön, M. Mayor, T. Wandlowski, and F. Pauly, Phys Rev B **85**, 075417 (2012).

[120] A. Migliore and A. Nitzan, ACS Nano **5**, 6669 (2011).

[121] A. Mishchenko, D. Vonlanthen, V. Meded, M. Burkle, C. Li, I. V. Pobelov, A. Bagrets, J. K. Viljas, F. Pauly, F. Evers, M. Mayor, and T. Wandlowski, Nano Lett. **10**, 156 (2010).

[122] J. Zhou, S. Samanta, C. Guo, J. Locklin, and B. Xu, Nanoscale **5**, 5715 (2013).

[123] K. Doi, M. Tsutsui, T. Ohshiro, C.-C. Chien, M. Zwolak, M. Taniguchi, T. Kawai, S. Kawano, and M. Di Ventra, J Phys Chem C **118**, 3758 (2014).

[124] R. N. Barnett, C. L. Cleveland, A. Joy, U. Landman, and G. B. Schuster, Science **294**, 567 (2001).

[125] J. M. Soler, E. Artacho, J. D. Gale, A. García, J. Junquera, P. Ordejón, and D. Sánchez-Portal, J. Phys.: Condens. Matter **14**, 2745 (2002).

[126] V. V. Zakjevskii, S. J. King, O. Dolgounitcheva, V. G. Zakrzewski, and J. V. Ortiz, J. Am. Chem. Soc. **128**, 13350 (2006).

[127] M. Tsutsui, M. Taniguchi, and T. Kawai, Nano Lett. **8**, 3293 (2008).

[128] A. M. Nowak and R. L. McCreery, J. Am. Chem. Soc. **126**, 16621 (2004).

[129] J.-H. Tian, B. Liu, Li, Z.-L. Yang, B. Ren, S.-T. Wu, Tao, and Z.-Q. Tian, J. Am. Chem. Soc. **128**, 14748 (2006).

[130] D. R. Ward, G. D. Scott, Z. K. Keane, N. J. Halas, and D. Natelson, J. Phys.: Condens. Matter **20**, 374118 (2008).

[131] M. R. Calvo, J. Fernandez-Rossier, J. J. Palacios, D. Jacob, D. Natelson, and C. Untiedt, Nature **458**, 1150 (2009).

[132] J. J. Parks, A. R. Champagne, G. R. Hutchison, S. Flores-Torres, H. D. Abruña, and D. C. Ralph, Phys. Rev. Lett. **99**, 026601 (2007).

[133] J. Zhou, F. Chen, and B. Xu, J. Am. Chem. Soc. **131**, 10439 (2009).

[134] B. Q. Xu, X. L. Li, X. Y. Xiao, H. Sakaguchi, and N. J. Tao, Nano Lett. **5**, 1491 (2005).

[135] S. S. Mallajosyula and S. K. Pati, J Phys Chem Lett **1**, 1881 (2010).

[136] L. Fang, J. Liu, S. Coulter, X. Cao, M. P. Schwartz, C. Hacker, and R. J. Hamers, Surface Science **514**, 362 (2002).

[137] R. L. McCreery, J. Wu, and R. P. Kalakodimi, Phys. Chem. Chem. Phys. **8**, 2572 (2006).

[138] P. G. Piva, G. A. DiLabio, J. L. Pitters, J. Zikovsky, M. Rezeq, S. Dogel, W. A. Hofer, and R. A. Wolkow, Nature **435**, 658 (2005).

[139] Z. J. Donhauser, B. A. Mantooth, K. F. Kelly, L. A. Bumm, J. D. Monnell, J. J. Stapleton, D. W. Price, A. M. Rawlett, D. L. Allara, J. M. Tour, and P. S. Weiss, Science **292**, 2303 (2001).

[140] J. A. Malen, P. Doak, K. Baheti, T. D. Tilley, A. Majumdar, and R. A. Segalman, Nano Lett. **9**, 3406 (2009).

[141] G. K. Ramachandran, T. J. Hopson, A. M. Rawlett, L. A. Nagahara, A. Primak, and S. M. Lindsay, Science **300**, 1413 (2003).

[142] J. Zhou, C. Guo, and B. Xu, J. Phys.: Condens. Matter **24**, 164209 (2012).

[143] S. Wu, M. T. González, R. Huber, S. Grunder, M. Mayor, C. Schönenberger, and M. Calame, Nature Nanotechnology **3**, 569 (2008).

[144] H. Vazquez, R. Skouta, S. Schneebeli, M. Kamenetska, R. Breslow, L. Venkataraman, and M. S. Hybertsen, Nature Nanotechnology **7**, 663 (2012).

[145] J.-C. Meiners and S. R. Quake, Phys. Rev. Lett. **84**, 5014 (2000).

[146] Y. Murayama, Y. Yogiashi, T. Iwamoto, Y. Mitsuhashi, and H. Homma, AIP Conference Proceedings **1518**, 619 (2013).

[147] A. Halbritter, P. Makk, S. Mackowiak, S. Csonka, M. Wawrzyniak, and J. Martinek, Phys. Rev. Lett. **105**, 266805 (2010).

[148] C. A. Martin, D. Ding, H. S. J. van der Zant, and J. M. van Ruitenbeek, New Journal of Physics **10**, 065008 (2008).

[149] K. Horiguchi, S. Kurokawa, and A. Sakai, J. Chem. Phys. **131**, 104703 (2009).

[150] Y.-C. Chen, M. Zwolak, and M. Di Ventra, Nano Lett. **4**, 1709 (2004).

[151] J. H. van de Sande, L. P. McIntosh, and T. M. Jovin, EMBO J. **1**, 777 (1982).

[152] A. Krzyaniak, P. Salaski, J. Jurczak, and J. Barciszewski, {FEBS} Letters **279**, 1 (1991).

[153] K. Siriwong and A. A. Voityuk, J. Phys. Chem. B **112**, 8181 (2008).

[154] J. H. van de Sande and T. M. Jovin, EMBO J. **1**, 115 (1982).

[155] T. Miyahara, H. Nakatsuji, and H. Sugiyama, J Phys Chem A **117**, 42 (2013).

[156] P. Várnai and Y. Timsit, Nucleic Acids Res. **38**, 4163 (2010).

[157] F. J. Ramírez, T. J. Thomas, T. Antony, J. Ruiz-Chica, and T. Thomas, Biopolymers **65**, 148 (2002).

[158] S. Zavriev, L. Minchenkova, M. Vorličková, A. Kolchinsky, M. Volkenstein, and V. Ivanov, Biochimica et Biophysica Acta (BBA) - Nucleic Acids and Protein Synthesis **564**, 212 (1979).

[159] L. Venkataraman, J. E. Klare, C. Nuckolls, M. S. Hybertsen, and M. L. Steigerwald, Nature **442**, 904 (2006).

[160] I. Franco, C. B. George, G. C. Solomon, G. C. Schatz, and M. A. Ratner, J. Am. Chem. Soc. **133**, 2242 (2011).

Appendix A

2D Correlation Histogram Algorithm

A.1 Pearson's Correlation Coefficient

Pearson's familiar formula for crosscorrelation is described in Section 3.3.3. In short, the crosscorrelation between two time-dependent variables is the scaled covariance between them. The poignant feature, as can be seen in Eq. 3.5, is the denominator which effectively scales the covariance based on the scale and units of the two variables. This not only allows for small changes in conductrance to be compared to larger changes in force, but also removes the units so that the resulting value for a force-conductance pair is unitless, and lies between $[-1, 1]$. As stated in the text, to achieve the formula for autocorrelation, it is only necessary to replace the force variable with the conductance variable. Thus, when in this appendix the crosscorrelation is described, so too is the autocorrelation.

The algorithm for producing the FC-2DCCH is shown as a flow chart in Fig. A.1. Broad strokes, the algorithm requires the data to be processed in the following steps:

1. Read in data

2. Clip data down to area of interest

3. Create 1D histograms of individual traces

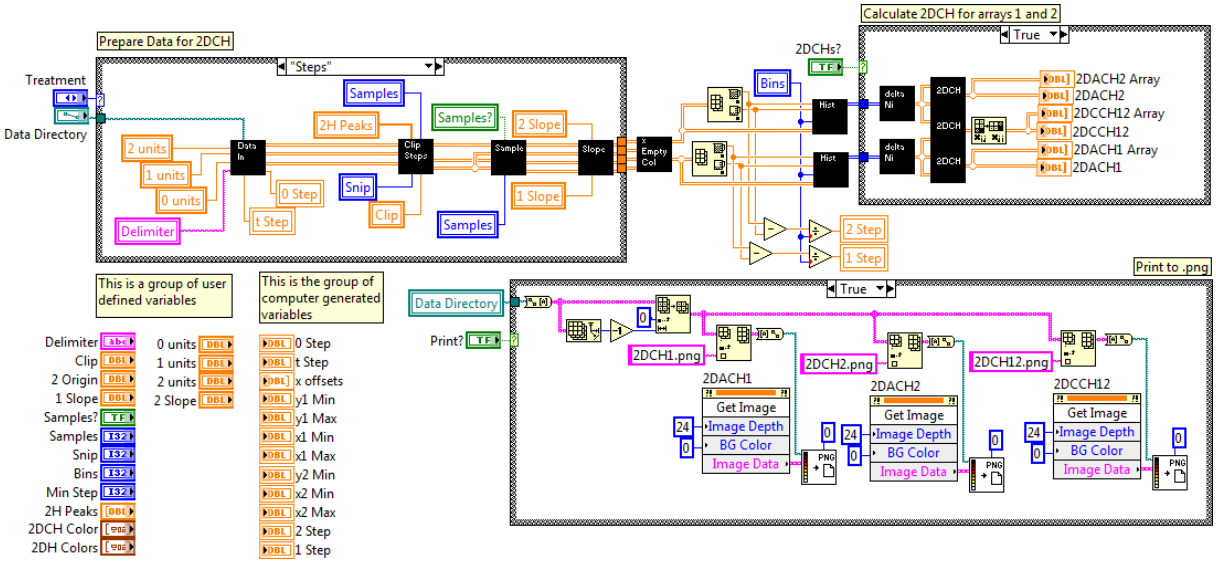

Figure A.1: Flow chart of entire algorithm which reads in the [t,F,C] data files, calculates the FC-2DCCH, and plots it.

4. Calculate crosscorrelation of traces

5. Plot, and

6. Print FC-2DCCH

Item 4 above is the meat of the algorithm, and is contained within the boolean block in the upper right corner of Fig. A.1, where the black boxes represent the subroutines shown in Fig. A.2. The subroutine in Fig. A.2a reads in the histograms as a block array of size $R \times N$, where R is the total number of traces in the data set, and N is the user-defined number of bins in the histograms. Because bin i of each trace histogram is data counts in a unique range of the variable, column i of the array of histograms for that variable is the same bin for all traces. The mean of this column is the average data counts for that bin or

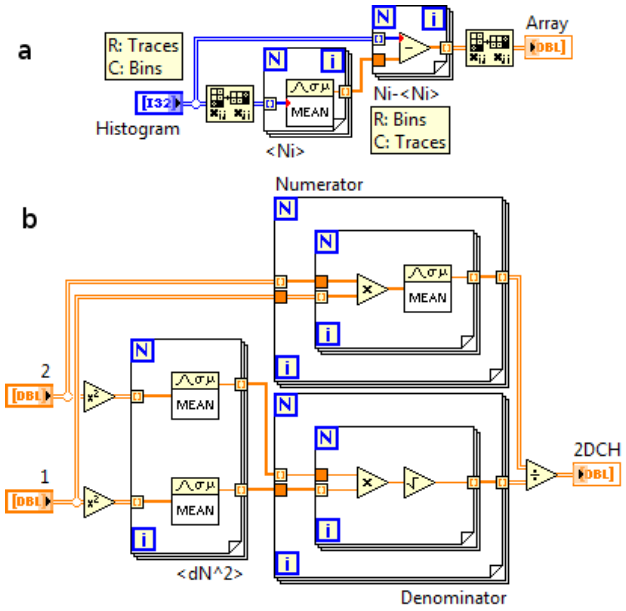

Figure A.2: Subroutines which compute the FC-2DCCH.

range of the variable. Subtracting this mean from element i of each trace histogram begins the process of calculating the covariance and the standard deviation. These variances for variables *1* and *2* are passed out of the subroutine in Fig. A.2a and into Fig. A.2b.

In the subroutine shown in Fig. A.2b the numerator and denominator of Eq. 3.5 are calculated. The denominator is essentially the standard deviation for each of the variables at bins i and j. The numerator is the covariance for each of the variables at bins i and j.

Because the calculation is made for each variable at bins i and j, the output is a single value for each locus *(i,j)* and accounts for the ability to plot this calculation on a 2D intensity plot.

The rest is to interpret the results. The first features to notice in Fig. 3.6 is that when autocorrelation is being calculated for a single variable, the 2D histogram is symmetric about the diagonal, and the diagonal is always 1. This is reasonable, because each 1D histogram

is perfectly correlated with itself, and *(i,j)=(j,i)*. These two features are not present in the crosscorrelation plots because force bin i is not perfectly correlated to conductance bin i in the same trace.

Were this method be developed more maturely, a complete description of the null hypothesis would be necessary to distinguish between acceptable noise variation in the data, and statistical artifacts that bear no physical significance.